Performance Analysis of STAR-RIS-Assisted Cell-Free Massive MIMO Systems with Electromagnetic Interference and Phase Errors

Jun Qian, *Member, IEEE,* Ross Murch, *Fellow, IEEE,* and Khaled B. Letaief, *Fellow, IEEE*

Abstract—Simultaneous Transmitting and Reflecting Reconfigurable Intelligent Surfaces (STAR-RISs) are being explored for the next generation of sixth-generation (6G) networks. A promising configuration for their deployment is within cell-free massive multiple-input multiple-output (MIMO) systems. However, despite the advantages that STAR-RISs could bring, challenges such as electromagnetic interference (EMI) and phase errors may lead to significant performance degradation. In this paper, we investigate the impact of EMI and phase errors on STAR-RIS-assisted cell-free massive MIMO systems and propose techniques to mitigate these effects. We introduce a novel projected gradient descent (GD) algorithm for STAR-RIS coefficient matrix design by minimizing the local channel estimation normalised mean square error. We also derive the closed-form expressions of the uplink and downlink spectral efficiency (SE) to analyze system performance with EMI and phase errors, in which fractional power control methods are applied for performance improvement. The results reveal that the projected GD algorithm can effectively tackle EMI and phase errors to improve estimation accuracy and compensate for performance degradation with nearly $10\% \sim 20\%$ SE improvement. Moreover, increasing access points (APs), antennas per AP, and STAR-RIS elements can also improve SE performance. Applying STAR-RIS in the proposed system achieves a larger 25%-likely SE than conventional RISs. However, the advantages of employing more STAR-RIS elements are reduced when EMI is severe.

Index Terms—Cell-free massive multiple-input multiple-output, electromagnetic interference, phase errors, simultaneous transmitting and reflecting reconfigurable intelligent surface, spatial correlation, spectral efficiency.

I. INTRODUCTION

THERE is a growing interest in researching sixth-generation (6G) wireless communication to address the ever-increasing demand for ubiquitous connectivity and higher data rates [1]–[4]. In past developments, massive multiple-input multiple-output (MIMO) has been one of the cornerstone technologies for enhancing data rates, reliability and coverage [5]–[7]. However, in cellular networks with cell boundaries, massive MIMO experiences harsh inter-cell interference [3].

To address the limit of massive MIMO in cellular networks, cell-free massive MIMO has been proposed to help diminish inter-cell interference, provide more extensive coverage and leverage favorable propagation configurations [8]–[10]. Cell-free massive MIMO utilizes a distributed architecture with

a central processing unit (CPU) that facilitates numerous geographically distributed access points (APs), which can synchronously provide service to users [3], [11], [12]. Cell-free massive MIMO integrates distributed networks and massive MIMO, so that the spectral efficiency (SE) performance can be greatly enhanced, even while using conjugate beamforming [2], [5], [13]. In [7], [11], a CPU-based large-scale fading decoding (LSFD) receiver has been proposed for uplink SE performance enhancement to utilize the benefits of cell-free massive MIMO. However, more APs introduce higher network overhead and power consumption, and the proposed system can experience poor quality of service (QoS) under severe propagation conditions [3], [7], [8]. Therefore, advanced technologies must be developed to meet the required QoS and handle these challenges in cell-free massive MIMO.

Reconfigurable intelligent surfaces (RISs) can be used to shape electromagnetic waves smartly without increasing the number of APs or power consumption. They are thus regarded as a promising technology to assist cell-free massive MIMO systems [5], [8], [14]. RISs are two-dimensional structures containing numerous passive reflecting elements that have the potential to reshape the propagation environment using the amplitude and phase shift adjustment at the RIS surface. RISs also do not need digital signal processing or active power amplifiers, so they can be implemented with lower complexity than a regular massive MIMO base station [13], [15], [16]. RISs can enhance wireless network performance by introducing additional controllable and reconfigurable cascaded links with low cost and power consumption [3], [6], [17]. Integrating RIS with cell-free massive MIMO could allow the advantages of both to be obtained jointly [18]–[20]. For example, the SE performance of spatially correlated RIS-assisted cell-free massive MIMO systems has been investigated [19], [21]. In [6], [18], [22], channel estimation improvement methods were introduced. [23] introduced hybrid beamforming for energy efficiency (EE) optimization to enhance RIS-assisted cell-free massive MIMO system performance. Moreover, [7], [22] evaluated the system performance of electromagnetic interference (EMI)-aware RIS-assisted cell-free massive MIMO and [13] studied the performance of RIS-assisted cell-free massive MIMO systems with channel aging and EMI.

In their conventional form, RIS is configured to reflect incoming signals, and therefore, in wireless configurations, the receiver and transmitter are located on the same side of the RIS [5], [24]. However, in practice, users may be positioned on both RIS sides [1], [5]. To tackle this limitation, [25],

[26] introduced the novel simultaneously transmitting and reflecting RIS (STAR-RIS) concept. STAR-RISs can provide full space coverage since the incoming signals incident on the STAR-RIS could be separated into reflected and transmitted signals [1], [5]. Moreover, the amplitudes and phases of the reflected and transmitted signals can be controlled by reflection and transmission coefficients, respectively, of the STAR-RIS [1], [5], [27]. To realize the benefits of STAR-RISs, [28] investigated the fundamental coverage characterization. [29] introduced passive beamforming design and resource allocation to optimize the sum rate and coverage range of STAR-RIS-assisted orthogonal multiple access (OMA) and non-orthogonal multiple access (NOMA) networks. STAR-RIS was also introduced in [30] to enhance full-duplex communication system performance. [27], [31] formulated a STAR-RIS-assisted massive MIMO system model to study the performance with phase errors introduced in [32], [33] caused by unavoidable phase-estimation imperfections.

Motivated by the interplay of RISs and cell-free massive MIMO systems, the joint benefits of STAR-RISs and cell-free massive MIMO systems may also be exploited [5]. Research on STAR-RIS-assisted cell-free massive MIMO systems is at an early stage. It includes [5], which introduced spatial correlation, and [24], which studied the sum-rate optimization of STAR-RIS-assisted cell-free massive MIMO systems. [21] studied the SE performance of active STAR-RIS-assisted cell-free massive MIMO systems considering spatial correlation. Similar to conventional RIS-assisted systems [7], [22], [34], [35], when STAR-RIS elements are highly correlated, EMI impinging on the STAR-RIS will degrade system performance. However, no existing analyses focus on EMI-aware STAR-RIS-assisted cell-free massive MIMO systems. This includes the absence of the analysis of performance limits and the introduction of design guidelines for STAR-RIS-assisted networks suffering from EMI. Moreover, as far as we know, the study of STAR-RIS/RIS-assisted cell-free massive MIMO with phase errors has also been limited with [27], [31] introducing the non-negligible phase error effect on STAR-RIS-assisted massive MIMO systems. Motivated by these observations, it is useful to analyze the joint effect of EMI and phase errors on the performance of STAR-RIS-assisted cell-free massive MIMO systems over spatially correlated channels.

To the best of our knowledge, this paper is the first to focus on the performance analysis of spatially correlated STAR-RIS-assisted cell-free massive MIMO systems, where STAR-RISs are non-ideal and experience EMI and phase errors. We derive the data transmission model and the closed-form expressions of the uplink and downlink SE with corresponding fractional power control. We introduce a projected gradient descent (GD) algorithm to enhance the channel estimation normalised mean square error (NMSE) and reduce the performance degradation caused by EMI and phase errors. Uplink transmission utilizes the LSFD at CPU and maximum ratio (MR) at APs. Additionally, downlink transmission applies conjugate beamforming. We also evaluate the sum SE performance with fractional power control methods.

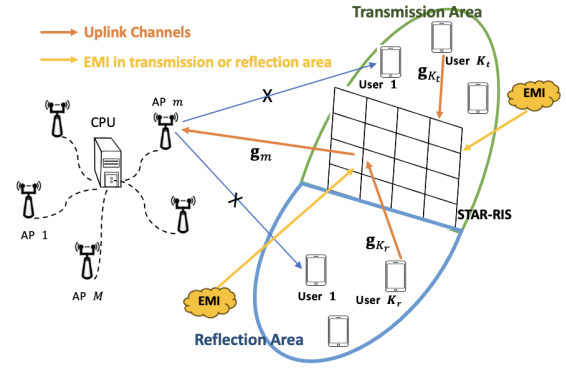In the following, we summarize the major contributions of this work as:

Fig. 1. System model for STAR-RIS-Assisted Cell-Free Massive MIMO Systems.

• We establish a spatially correlated STAR-RIS-assisted cell-free massive MIMO model with EMI and phase errors. To the best of our knowledge, this is the first work to introduce EMI and phase errors in STAR-RIS-assisted cell-free massive MIMO.

• To investigate the impact of EMI and phase errors on the proposed system performance, we derive the data transmission model and the closed-form expressions of uplink and downlink SE with corresponding fractional power control. We then conduct Monte Carlo simulations to validate the closed-form analytical results.

• We propose a projected GD algorithm for the uplink channel estimation to optimize the STAR-RIS coefficient matrix, which contains the optimization of the amplitudes and the phase shifts of the STAR-RIS. Our proposed GD algorithm can minimize the channel estimation NMSE and introduce extra channel estimation accuracy gain.

• The results show that the proposed GD algorithm, more APs, and antennas per AP could compensate for the performance degradation brought on by EMI and phase errors. Moreover, more STAR-RIS elements are required to improve system performance, while STAR-RISs cannot bring significant gain when EMI is severe.

The remainder of this paper is organized as follows. Section II introduces the spatially correlated STAR-RIS-assisted channel model with EMI and phase errors. Section III introduces uplink channel estimation with pilot contamination and the projected GD algorithm. Section IV and Section V derive closed-form analytical expressions for the uplink and downlink SE with fractional power control, respectively. We provide numerical results and discussions in Section VI, and Section VII summarizes the paper and proposes subsequent works.

II. SYSTEM MODEL

Fig. 1 illustrates a STAR-RIS-assisted cell-free massive MIMO system [5], [21]. M APs with N antennas each, connected to the CPU through optimal backhaul links, can serve K single-antenna users synchronously. The L-element STAR-RIS assists in the communication between APs and users. First, the group of users indexed by set $\mathcal{K}_r$ with cardinality $|\mathcal{K}_r| = K_r$, are located on the same side of the APs and STAR-RIS in the reflection area. Similarly, users indexed by set $\mathcal{K}_t$ with

$|\mathcal{K}_t| = K_t$, are located in the transmission area of the STAR-RIS. Note that $K_r + K_t = K$ and $\mathcal{K}_r \cap \mathcal{K}_t = \varnothing$. We also define the STAR-RIS operation mode of the k-th user as ω_k, $\forall k$. That is, if the k-th user is located in the reflection area experiencing the reflection mode of the STAR-RIS ($k \in \mathcal{K}_r$), $\omega_k = r$. Similarly, $\omega_k = t$ if the k-th user is located in the transmission area experiencing the transmission mode of the STAR-RIS ($k \in \mathcal{K}_t$) [5]. Moreover, $\mathcal{W}_k$ is the set of users sharing the same STAR-RIS operation mode, including the k-th user.

A. STAR-RIS Protocols

In general, energy splitting (ES), mode switching (MS), and time switching (TS) have been introduced as three feasible protocols for STAR-RIS operation [1], [5]. In this work, we mainly focus on ES protocol, in which all STAR-RIS elements are operated jointly in reflection and transmission modes to serve all users regardless of their locations. As such, the STAR-RIS coefficient matrices follow $\mathbf{\Theta}_t = \text{diag}(u_1^t \theta_1^t, u_2^t \theta_2^t, ..., u_L^t \theta_L^t) \in \mathbb{C}^{L \times L}$ for the transmission mode and $\mathbf{\Theta}_r = \text{diag}(u_1^r \theta_1^r, u_2^r \theta_2^r, ..., u_L^r \theta_L^r) \in \mathbb{C}^{L \times L}$ for the reflection mode, respectively, where ES amplitude coefficients are u_l^t, $u_l^r \in [0, 1]$, $(u_l^t)^2 + (u_l^r)^2 = 1$, and the induced phase shifts are $\theta_l^t = e^{i\varphi_l^t}$, $\theta_l^r = e^{i\varphi_l^r}$ with φ_l^t, $\varphi_l^r \in [0, 2\pi)$, $\forall l$ [1], [21]. Note that the consideration that the reflecting coefficient phase and transmitting coefficient phase are coupled is left for future works [5]. Moreover, it is possible to treat the MS protocol as a special case of ES protocol, in which u_l^t, u_l^r are restricted to binary values, namely u_l^t, $u_l^r \in \{0, 1\}$ [1], [5].

B. STAR-RIS-assisted Channel Model with Phase Errors

We assume that the system experiences correlated Rayleigh fading and operates in time-division duplex (TDD) mode [13], [15], [36], experiencing channel reciprocity. This work assumes that obstacles have blocked the direct channels between the k-th user and the m-th AP. In this case, only the cascaded STAR-RIS-assisted channels are available for communication [5]. The cascaded STAR-RIS-assisted uplink channel between the k-th user and the m-th AP can be provided by

$$\mathbf{g}_{mk} = \mathbf{g}_m \bar{\mathbf{\Theta}}_{\omega_k} \mathbf{\Theta}_{\omega_k} \mathbf{g}_k, \tag{1}$$

where $\mathbf{\Theta}_{\omega_k}$ is the STAR-RIS coefficient matrix defined in Sec. II-A. The phase error matrix is defined as $\bar{\mathbf{\Theta}}_{\omega_k} = \text{diag}(\bar{\theta}_1^{\omega_k}, \bar{\theta}_2^{\omega_k}, ..., \bar{\theta}_L^{\omega_k}) \in \mathbb{C}^{L \times L}$, where $\bar{\theta}_l^{\omega_k} = e^{i\bar{\varphi}_l^{\omega_k}}$, $\forall l$, $\forall k$. Note that the phase errors are typically modelled by independent and identically distributed (i.i.d) random variables with a zero mean satisfying the uniform distribution or the von Mises distribution [27], [33], [37]. In this paper, we consider $\bar{\varphi}_l^{\omega_k} \in [-a, a]$, $\forall l$, following the uniform distribution with zero mean and a characteristic function as $\mathbb{E}\{e^{i\bar{\varphi}_l^{\omega_k}}\} = \frac{\sin(a)}{a} = \phi$, $\forall l$ [31], [37]. Furthermore, the uplink channel from the STAR-RIS to the m-th AP, $\mathbf{g}_m \in \mathbb{C}^{N \times L}$, is obtained as

$$\mathbf{g}_m = \sqrt{\beta_m} \mathbf{R}_{m,r}^{1/2} \mathbf{v}_m \mathbf{R}_{m,t}^{1/2}, \tag{2}$$

where β_m is the large-scale fading coefficient between the m-th AP and the STAR-RIS, $\mathbf{v}_m \in \mathbb{C}^{N \times L}$ consists of i.i.d. random variables following $\mathcal{CN}(0, 1)$. The respective spatial

correlation matrices at the m-th AP and STAR-RIS are $\mathbf{R}_{m,r}$ and $\mathbf{R}_{m,t} = A\mathbf{R} \in \mathbb{C}^{L \times L}$ [5], [13], [22]. In particular, d_H and d_V are the respective horizontal width and the vertical height to introduce the STAR-RIS element area $A = d_H d_V$ [38]. The (x, y)-th element in $\mathbf{R}$ is given by [35]

$$[\mathbf{R}]_{x,y} = \text{sinc}\left(\frac{2\|\mathbf{e}_x - \mathbf{e}_y\|}{\lambda_c}\right), \tag{3}$$

where $\text{sinc}(a) = \sin(\pi a)/(\pi a)$ is the sinc function, λ_c is the carrier wavelength [7], [19], [35]. The position vector of the x-th STAR-RIS element is $\mathbf{e}_x = [0, \text{mod}(x - 1, L_h)d_h, \lfloor(x - 1)/L_h\rfloor d_v]^T$ [7], [13]. L_h is the number of column elements and L_v is the number of row elements at STAR-RIS, with $L = L_h L_v$. Moreover, the uplink channel between the k-th user and the STAR-RIS, $\mathbf{g}_k \in \mathbb{C}^{L \times 1}$ is formulated as

$$\mathbf{g}_k = \sqrt{\beta_k} \mathbf{R}_k^{1/2} \mathbf{v}_k. \tag{4}$$

Similar to (2), β_k is the large-scale fading coefficient between the k-th user and the STAR-RIS. $\mathbf{R}_k = A\mathbf{R} \in \mathbb{C}^{L \times L}$ is the spatial correlation matrix of STAR-RIS following (3). $\mathbf{v}_k \in \mathbb{C}^{L \times 1}$ is the independent fast-fading channel containing i.i.d random variables obeying $\mathcal{CN}(0, 1)$. In this case, the channel vector $\mathbf{g}_{mk}$ has the covariance matrix distributed as

$$\begin{aligned}
\mathbf{\Delta}_{mk} &= \mathbb{E}\{\mathbf{g}_{mk}\mathbf{g}_{mk}^H\} \\
&= \beta_m \beta_k \mathbf{R}_{m,r} \text{tr}\left(\mathbf{R}_{m,t}^{1/2} \bar{\mathbf{\Theta}}_{\omega_k} \mathbf{\Theta}_{\omega_k} \mathbf{R}_k \mathbf{\Theta}_{\omega_k}^H \bar{\mathbf{\Theta}}_{\omega_k}^H \mathbf{R}_{m,t}^{1/2}\right) \\
&= \beta_m \beta_k \mathbf{R}_{m,r} \text{tr}(\mathbf{T}_{\omega_k}),
\end{aligned} \tag{5}$$

with

$$\mathbf{T}_{\omega_k} = A^2 \mathbf{R}^{1/2} \bar{\mathbf{\Theta}}_{\omega_k} \mathbf{\Theta}_{\omega_k} \mathbf{R} \mathbf{\Theta}_{\omega_k}^H \bar{\mathbf{\Theta}}_{\omega_k}^H \mathbf{R}^{1/2} = A^2 \mathbf{R}^{1/2} \bar{\mathbf{R}}_{\omega_k} \mathbf{R}^{1/2}, \tag{6}$$

where $\bar{\mathbf{R}}_{\omega_k} = \mathbb{E}\{\bar{\mathbf{\Theta}}_{\omega_k} \mathbf{\Theta}_{\omega_k} \mathbf{R} \mathbf{\Theta}_{\omega_k}^H \bar{\mathbf{\Theta}}_{\omega_k}^H\} = \mathbb{E}\{\mathbf{\Theta}_{\omega_k} \bar{\mathbf{\Theta}}_{\omega_k} \mathbf{R} \bar{\mathbf{\Theta}}_{\omega_k}^H \mathbf{\Theta}_{\omega_k}^H\} = \mathbf{\Theta}_{\omega_k}\left(\phi^2 \mathbf{R} + (1 - \phi^2)\mathbf{R} \circ \mathbf{I}_L\right)\mathbf{\Theta}_{\omega_k}^H$ [27], [31]. Since we consider the uniformly distributed phase errors, $\mathbf{\Delta}_{mk}$ does not depend on the phase-shifts if $\phi = 0$ [27]. For ease of calculation, we assume that $a = \pi/2$ in this paper to study the STAR-RIS coefficient optimization. The von Mises-distributed phase errors will be studied in future works.

C. Electromagnetic Interference Model

Based on [35], successive incoming plane waves introduced by external sources can superpose to generate EMI to degrade the system performance. The electromagnetic waves are typically incident from directions spanning large angular intervals [7], [13], [35]. Then, the STAR-RIS spatial correlation model applies to uniform-distributed isotropic scattering [3], [35]. The EMI impinging on the STAR-RIS can be given by

$$\mathbf{n}_\omega \sim \mathcal{CN}(0, A\sigma_\omega^2 \mathbf{R}), \tag{7}$$

where $\omega = t$, r represents the transmission or reflection area EMI comes from, σ_ω^2 is the EMI power in the relevant area. We introduce a modified EMI power expression referring to [7], [13], [35] to make the EMI scalable and feasible. First, when $\omega = r$, the EMI in the reflection area has the power

$$\sigma_r^2 = \sqrt{\frac{p_u p_d \sum_{m=1}^M \beta_m \sum_{k \in \mathcal{K}_r} \beta_k}{M K_r \rho_r^2}}, \tag{8}$$

where p_d and p_u are the respective downlink and user transmit power. ρ_r is the ratio of the received signal power and the EMI power in the STAR-RIS reflection area [7], [35]. Similarly, when $\omega = t$, the EMI in the transmission area has the power

$$\sigma_t^2 = \frac{p_u \sum_{k \in \mathcal{K}_t} \beta_k}{K_t \rho_t}, \tag{9}$$

where ρ_t represents the ratio of the received signal power and the EMI power in the STAR-RIS transmission area. For simplicity, $\rho_t = \rho_r = \rho$ is assumed in this work.

III. UPLINK CHANNEL ESTIMATION UTILIZING THE PROJECTED GD ALGORITHM

We propose a projected GD algorithm that minimizes the channel estimation NMSE to optimize the STAR-RIS coefficient matrix. The optimization of the STAR-RIS coefficient matrix is crucial since improving the channel estimation accuracy results in notable performance enhancement [3], [5]. In our approach, we adopt the cascaded channel estimation with an uplink channel estimation phase using pilot symbols [5].

A. Uplink Channel Estimation

For uplink channel estimation, $\sqrt{\tau_p}\varphi_k \in \mathbb{C}^{\tau_p \times 1}$ is assumed to be the pilot sequence allocated to k-th user, in which τ_p is the pilot signal length and $\varphi_k^H \varphi_k = 1, \forall k$. Note that τ_c, the coherence interval, is much larger than τ_p for higher transmission efficiency [3], [7]. In this case, $K > \tau_p$ introduces users sharing the same orthogonal pilot sequences and results in pilot contamination [12]. We adopt $\mathcal{P}_k$ with $\varphi_k^H \varphi_{k'} = 1, \forall k' \in \mathcal{P}_k$, to represent the user set using the same pilot sequence including k itself. Distinct from the conventional assumption [3], [6], we consider that EMIs from the reflection area and transmission area impinging on the STAR-RIS jointly are received by APs in the channel estimation phase [7], [35]. Thus, we can obtain the received signal at m-th AP, $\mathbf{Y}_{m,p} \in \mathbb{C}^{N \times \tau_p}$, as

$$\mathbf{Y}_{m,p} = \sqrt{\tau_p p_p} \sum_{k=1}^{K} \mathbf{g}_{mk}\varphi_k^H + \mathbf{g}_m \bar{\mathbf{\Theta}}_r \mathbf{\Theta}_r \mathbf{N}_r + \mathbf{g}_m \bar{\mathbf{\Theta}}_t \mathbf{\Theta}_t \mathbf{N}_t + \mathbf{N}_{m,p}, \tag{10}$$

where p_p is the pilot transmit power, $\mathbf{N}_r$ and $\mathbf{N}_t$ are the respective EMI from the reflection area and transmission area, with v-th column following $\left[\mathbf{N}_\omega\right]_v \sim \mathcal{CN}(\mathbf{0}, A\sigma_\omega^2 \mathbf{R})$, $\omega \in \{t, r\}$. $\mathbf{N}_{m,p}$ is the additive white Gaussian noise (AWGN), where v-th column follows $\left[\mathbf{N}_{m,p}\right]_v \sim \mathcal{CN}(\mathbf{0}, \sigma^2 \mathbf{I}_N)$, in which σ^2 is the noise power. Then, the projection of $\mathbf{Y}_{m,p}$ on φ_k is given by

$$\begin{aligned}
\mathbf{y}_{mk,p} &= \mathbf{Y}_{m,p}\varphi_k \\
&= \sqrt{\tau_p p_p} \sum_{k'=1}^{K} \mathbf{g}_{mk'}\varphi_{k'}^H \varphi_k \\
&\quad + \mathbf{g}_m \bar{\mathbf{\Theta}}_r \mathbf{\Theta}_r \mathbf{N}_r \varphi_k + \mathbf{g}_m \bar{\mathbf{\Theta}}_t \mathbf{\Theta}_t \mathbf{N}_t \varphi_k + \mathbf{N}_{m,p}\varphi_k \\
&= \sqrt{\tau_p p_p} \sum_{k' \in \mathcal{P}_k} \mathbf{g}_{mk'} + \mathbf{g}_m \bar{\mathbf{\Theta}}_r \mathbf{\Theta}_r \mathbf{N}_r \varphi_k + \mathbf{g}_m \bar{\mathbf{\Theta}}_t \mathbf{\Theta}_t \mathbf{N}_t \varphi_k \\
&\quad + \mathbf{N}_{m,p}\varphi_k.
\end{aligned} \tag{11}$$

According to the minimum mean square error (MMSE) estimation method [13], [18], $\mathbf{g}_{mk}$ is estimated by

$$\hat{\mathbf{g}}_{mk} = \frac{\mathbb{E}\left\{\mathbf{y}_{mk,p}\mathbf{g}_{mk}^H\right\}}{\mathbb{E}\left\{\mathbf{y}_{mk,p}\mathbf{y}_{mk,p}^H\right\}}\mathbf{y}_{mk,p} = \sqrt{\tau_p p_p}\mathbf{\Delta}_{mk}\mathbf{\Psi}_{mk}^{-1}\mathbf{y}_{mk,p}, \tag{12}$$

where

$$\begin{aligned}
\mathbf{\Psi}_{mk} &= \tau_p p_p \sum_{k' \in \mathcal{P}_k} \mathbf{\Delta}_{mk'} \\
&\quad + \left(\beta_m \sigma_r^2 \text{tr}(\mathbf{T}_r) + \beta_m \sigma_t^2 \text{tr}(\mathbf{T}_t)\right)\mathbf{R}_{m,r} + \sigma^2 \mathbf{I}_N.
\end{aligned} \tag{13}$$

Based on the above-mentioned observations, the channel estimation $\hat{\mathbf{g}}_{mk}$ and the estimation error $\tilde{\mathbf{g}}_{mk} = \mathbf{g}_{mk} - \hat{\mathbf{g}}_{mk}$ can be distributed by $\mathcal{CN}(\mathbf{0}, \mathbf{Q}_{mk})$ and $\mathcal{CN}(\mathbf{0}, \mathbf{\Delta}_{mk} - \mathbf{Q}_{mk})$, respectively, with

$$\mathbf{Q}_{mk} = \tau_p p_p \mathbf{\Delta}_{mk}(\mathbf{\Delta}_{mk}\mathbf{\Psi}_{mk}^{-1})^H. \tag{14}$$

Then, referring to [6], [39], the channel estimation accuracy can be verified by the channel estimation NMSE, given by

$$\text{NMSE} = \frac{\sum_{m=1}^{M} \sum_{k=1}^{K} \mathbb{E}\left\{\|\tilde{\mathbf{g}}_{mk}\|^2\right\}}{\sum_{m=1}^{M} \sum_{k=1}^{K} \mathbb{E}\left\{\|\mathbf{g}_{mk}\|^2\right\}} = \frac{\sum_{m=1}^{M} \sum_{k=1}^{K} \text{tr}(\mathbf{\Delta}_{mk} - \mathbf{Q}_{mk})}{\sum_{m=1}^{M} \sum_{k=1}^{K} \text{tr}(\mathbf{\Delta}_{mk})}. \tag{15}$$

B. STAR-RIS Coefficient Matrix Optimization

To improve the channel estimation accuracy, we focus on minimizing the NMSE from all users and APs in (15) to optimize STAR-RIS coefficient matrices. First, we model the optimization problem for the NMSE minimization of STAR-RIS-assisted cell-free massive MIMO systems regarding phase shifts and amplitudes as [3], [5]

$$P_1: \min_{\theta, \mathbf{u}} \text{NMSE} \tag{16a}$$

subject to

$$(u_l^t)^2 + (u_l^r)^2 = 1, \ \forall l \tag{16b}$$

$$u_l^t \geq 0, \ u_l^r \geq 0, \ \forall l \tag{16c}$$

$$|\theta_l^t| = |\theta_l^r| = 1, \ \forall l \tag{16d}$$

where $\theta = [\theta_t, \theta_r]$ and $\mathbf{u} = [\mathbf{u}_t, \mathbf{u}_r]$. $\theta_\omega \in \mathbb{C}^{L \times L}$ and $\mathbf{u}_\omega \in \mathbb{C}^{L \times L}$ are diagonal matrices with $\mathbf{\Theta}_\omega = \mathbf{u}_\omega \theta_\omega = \theta_\omega \mathbf{u}_\omega$, $\omega \in \{r, t\}$. The optimization problem is non-convex [5], [40]. The amplitudes and the phase shifts for reflection and transmission are coupled [5]. Thus, we focus on the projected gradient descent (GD) algorithm to achieve the optimal solution to the minimization problem locally [40], [41]. The proposed projected GD algorithm, decreasing the objective from the current iteration $(\theta^n, \mathbf{u}^n)$ to the gradient direction, contains the following iterations [5], [42], [43]

$$\theta^{n+1} = \text{P}_\theta\left(\theta^n - \mu\nabla_{\theta^n}\text{NMSE}(\theta^n, \mathbf{u}^n)\right), \tag{17}$$

$$\mathbf{u}^{n+1} = \text{P}_\mathbf{u}\left(\mathbf{u}^n - \mu\nabla_{\mathbf{u}^n}\text{NMSE}(\theta^n, \mathbf{u}^n)\right), \tag{18}$$

where μ is the step size for θ and $\mathbf{u}$, the superscript is the iteration index. To meet the constraints, we apply the projection functions $\text{P}_\theta(\theta)$ and $\text{P}_\mathbf{u}(\mathbf{u})$ following [5], [44]

$$[\text{P}_\theta(\theta)]_{i,z} = \frac{\theta_{i,z}}{|\theta_{i,z}|}, \ z \in \{i, i+L\}, \ i = 1, ..., L, \tag{19}$$

$$[\text{P}_\mathbf{u}(\mathbf{u})]_{i,z} = \frac{\mathbf{u}_{i,z}}{\sqrt{\mathbf{u}_{i,i}^2 + \mathbf{u}_{i,i+L}^2}}, \ z \in \{i, i+L\}, \ i = 1, ..., L. \tag{20}$$

Based on the observations mentioned above, Algorithm 1 illustrates the iterative procedure of the projected GD algorithm to converge to a stationary point of P_1 [5], [40]. We initialize

$$\nabla_{\mathbf{x}_\omega}\text{NMSE}(\boldsymbol{\theta},\mathbf{u}) = \nabla_{\mathbf{x}_\omega}\frac{\sum_{m=1}^{M}\sum_{k=1}^{K}\text{tr}(\boldsymbol{\Delta}_{mk}-\mathbf{Q}_{mk})}{\sum_{m=1}^{M}\sum_{k=1}^{K}\text{tr}(\boldsymbol{\Delta}_{mk})}$$

$$= \frac{\sum_{m=1}^{M}\sum_{k=1}^{K}\text{tr}(\mathbf{Q}_{mk})\nabla_{\mathbf{x}_\omega}\left(\sum_{m=1}^{M}\sum_{k=1}^{K}\text{tr}(\boldsymbol{\Delta}_{mk})\right)-\sum_{m=1}^{M}\sum_{k=1}^{K}\text{tr}(\boldsymbol{\Delta}_{mk})\nabla_{\mathbf{x}_\omega}\left(\sum_{m=1}^{M}\sum_{k=1}^{K}\text{tr}(\mathbf{Q}_{mk})\right)}{\left(\sum_{m=1}^{M}\sum_{k=1}^{K}\text{tr}(\boldsymbol{\Delta}_{mk})\right)^2} \tag{24}$$

$$= \frac{\sum_{m=1}^{M}\sum_{k=1}^{K}\text{tr}(\mathbf{Q}_{mk})\cdot\left(\sum_{m=1}^{M}\sum_{k\in\mathcal{K}_\omega}\nabla_{\mathbf{x}_\omega}\text{tr}(\boldsymbol{\Delta}_{mk})\right)-\sum_{m=1}^{M}\sum_{k=1}^{K}\text{tr}(\boldsymbol{\Delta}_{mk})\left(\sum_{m=1}^{M}\sum_{k\in\mathcal{K}_\omega}\nabla_{\mathbf{x}_\omega}\text{tr}(\mathbf{Q}_{mk})\right)}{\left(\sum_{m=1}^{M}\sum_{k=1}^{K}\text{tr}(\boldsymbol{\Delta}_{mk})\right)^2},$$

$$\nabla_{\boldsymbol{\theta}_{\omega_k}}\text{tr}(\mathbf{Q}_{mk}) = A^2\tau_p p_p\text{tr}\left(\boldsymbol{\Psi}_{mk}^{-1}\boldsymbol{\Delta}_{mk}\boldsymbol{\Pi}_{mk}+\boldsymbol{\Delta}_{mk}\boldsymbol{\Psi}_{mk}^{-1}\boldsymbol{\Pi}_{mk}\right)\text{diag}\left(\bar{\mathbf{R}}\boldsymbol{\Theta}_{\omega_k}^*\mathbf{R}^T\mathbf{u}_{\omega_k}^T\right)$$
$$- A^2\tau_p p_p\left(\tau_p p_p\sum_{k'\in\mathcal{P}_k\cap\mathcal{W}_k}\text{tr}\left(\boldsymbol{\Psi}_{mk}^{-1}\boldsymbol{\Delta}_{mk}^2\boldsymbol{\Psi}_{mk}^{-1}\boldsymbol{\Pi}_{mk'}\right)\text{diag}\left(\bar{\mathbf{R}}\boldsymbol{\Theta}_{\omega_{k'}}^*\mathbf{R}^T\mathbf{u}_{\omega_{k'}}^T\right)-\beta_m\sigma_{\omega_k}^2\text{tr}\left(\boldsymbol{\Psi}_{mk}^{-1}\boldsymbol{\Delta}_{mk}^2\boldsymbol{\Psi}_{mk}^{-1}\mathbf{R}_{m,r}\right)\text{diag}\left(\bar{\mathbf{R}}\boldsymbol{\Theta}_{\omega_k}^*\mathbf{R}^T\mathbf{u}_{\omega_k}^T\right)\right). \tag{26}$$

Algorithm 1 Gradient Descent Based STAR-RIS Design

Inputs: ϵ (tolerance), IterMax;
Output: $\boldsymbol{\theta}$, $\mathbf{u}$, NMSE$(\boldsymbol{\theta},\mathbf{u})$
1: Initialize $\boldsymbol{\theta}^0$, $\mathbf{u}^0$, $\mathbf{f}^0 = \text{NMSE}(\boldsymbol{\theta}^0,\mathbf{u}^0)$
2: **for** t = 1 : IterMax **do**
3:     $\boldsymbol{\theta} = []$, $\mathbf{u} = []$;
4:     $\mu = 1 - \dfrac{t-1}{2\cdot\text{IterMax}}$;   (step size)
5:     $\boldsymbol{\theta} = \text{P}_{\boldsymbol{\theta}}\left(\boldsymbol{\theta}^0 - \mu\nabla_{\boldsymbol{\theta}^0}\text{NMSE}(\boldsymbol{\theta}^0,\mathbf{u}^0)\right)$
6:     $\mathbf{u} = \text{P}_{\mathbf{u}}\left(\mathbf{u}^0 - \mu\nabla_{\mathbf{u}^0}\text{NMSE}(\boldsymbol{\theta}^0,\mathbf{u}^0)\right)$
7:     Calculate $\mathbf{f} = \text{NMSE}(\boldsymbol{\theta},\mathbf{u})$
8:     **if** $\left|\mathbf{f}-\mathbf{f}^0\right|\leq\epsilon$ **then**
9:         **break**
10:    **else**
11:        $\boldsymbol{\theta}^0 = \boldsymbol{\theta}$, $\mathbf{u}^0 = \mathbf{u}$, $\mathbf{f}^0 = \mathbf{f}$;
12:    **end if**
13: **end for**

---

the step size μ and reduce it by increasing the iterations.
Proposition 1: When the MS protocol is in operation, for simplicity, the projected GD algorithm for $\mathbf{u}$ is updated to

$$\mathbf{u}^{n+1} = \bar{\text{P}}_{\mathbf{u}}\left(\nabla_{\mathbf{u}^n}\text{NMSE}(\boldsymbol{\theta}^n,\mathbf{u}^n)\right), \tag{21}$$

with $z\in\{i,i+L\}$, $\bar{\text{P}}_{\mathbf{u}}(\mathbf{u})$ is defined as

$$[\bar{\text{P}}_{\mathbf{u}}(\mathbf{u})]_{i,z} = \begin{cases} 1, & \max(|\mathbf{u}_{i,i}|,|\mathbf{u}_{i,i+L}|) = |\mathbf{u}_{i,z}| \\ 0, & \max(|\mathbf{u}_{i,i}|,|\mathbf{u}_{i,i+L}|) > |\mathbf{u}_{i,z}|. \end{cases} \tag{22}$$

Proposition 2: Note that the complex gradients of NMSE$(\boldsymbol{\theta},\mathbf{u})$ in terms of $\boldsymbol{\theta}$, $\mathbf{u}$ can be computed as [5], [42], [43]

$$\nabla_{\mathbf{x}}\text{NMSE}(\boldsymbol{\theta},\mathbf{u}) = [\nabla_{\mathbf{x}_t}\text{NMSE}(\boldsymbol{\theta},\mathbf{u})^T, \nabla_{\mathbf{x}_r}\text{NMSE}(\boldsymbol{\theta},\mathbf{u})^T]^T, \tag{23}$$

where $\mathbf{x}\in\{\boldsymbol{\theta},\mathbf{u}\}$. The decomposition of $\nabla_{\mathbf{x}_\omega}\text{NMSE}(\boldsymbol{\theta},\mathbf{u})^T$ is shown in (24) at the top of this page with $\omega\in\{t,r\}$. Similar to (6), $\bar{\mathbf{R}} = \mathbb{E}\{\bar{\boldsymbol{\Theta}}_{\omega_k}^T\mathbf{R}^T\bar{\boldsymbol{\Theta}}_{\omega_k}^*\} = \phi^2\mathbf{R}+(1-\phi^2)\mathbf{I}_L$. Referring to [45], [46], we can obtain the following closed-form expressions as

$$\nabla_{\boldsymbol{\theta}_{\omega_k}}\text{tr}(\boldsymbol{\Delta}_{mk}) = A^2\beta_m\beta_k\text{tr}\left(\mathbf{R}_{m,r}\right)\text{diag}\left(\bar{\mathbf{R}}\boldsymbol{\Theta}_{\omega_k}^*\mathbf{R}^T\mathbf{u}_{\omega_k}^T\right), \tag{25}$$

$$\nabla_{\mathbf{u}_{\omega_k}}\text{tr}(\boldsymbol{\Delta}_{mk}) = 2A^2\beta_m\beta_k\text{tr}\left(\mathbf{R}_{m,r}\right)\Re\mathfrak{E}\left\{\text{diag}\left(\bar{\mathbf{R}}\boldsymbol{\Theta}_{\omega_k}^*\mathbf{R}^T\boldsymbol{\theta}_{\omega_k}^T\right)\right\}, \tag{27}$$

and $\nabla_{\boldsymbol{\theta}_{\omega_k}}\text{tr}(\mathbf{Q}_{mk})$ and $\nabla_{\mathbf{u}_{\omega_k}}\text{tr}(\mathbf{Q}_{mk})$ are shown as (26) at the top of this page and (28) at the top of the next page.
Proof: Please see Appendix A.

As an overall summary, we can use (14) and (15) to determine the channel estimation NMSE by applying the projected GD algorithm with (17)-(18) to optimize (16).

IV. UPLINK TRANSMISSION AND CLOSED-FORM SE EXPRESSIONS

We derive novel closed-form uplink SE expressions with fractional power control to investigate the uplink performance of the proposed STAR-RIS-assisted cell-free massive MIMO systems. EMI and phase errors are included in the analysis. Local MR decoding at the APs and LSFD processing at the CPU during the uplink transmission are introduced [7], [13].

A. Uplink Data Transmission

First, APs use the local channel estimation to estimate the corresponding uplink data. Next, APs forward the data estimates to the CPU for data detection [12], [47]. Thus, the received signal at the m-th AP, $\mathbf{y}_m\in\mathbb{C}^{N\times 1}$ is obtained as

$$\mathbf{y}_m = \sqrt{p_u}\sum_{k=1}^{K}\mathbf{g}_{mk}\sqrt{\eta_k}s_k + \mathbf{g}_m\bar{\boldsymbol{\Theta}}_r\boldsymbol{\Theta}_r\mathbf{n}_r + \mathbf{g}_m\bar{\boldsymbol{\Theta}}_t\boldsymbol{\Theta}_t\mathbf{n}_t + \mathbf{w}_m, \tag{29}$$

where p_u is the user transmit power. $s_k\sim\mathcal{CN}(0,1)$ is the k-th user's transmit signal, η_k is the uplink power control coefficient with $\sum_{k=1}^{K}\eta_k\leq K$. $\mathbf{n}_\omega\sim\mathcal{CN}(0,A\sigma_\omega^2\mathbf{R})$ is the EMI at the reflection area or transmission area, with respect to $\omega\in\{t,r\}$. $\mathbf{w}_m\sim\mathcal{CN}(0,\sigma^2\mathbf{I}_N)$ is the noise at the m-th AP.

Then, the m-th AP multiplies its local channel estimate conjugate with $\mathbf{y}_m$ to detect the symbol transmitted by the k-th user. Subsequently, APs send the obtained quantity $\check{s}_{mk}\triangleq\hat{\mathbf{g}}_{mk}^H\mathbf{y}_m$ to the CPU via the fronthaul link [3], [13], [47]. The CPU uses weights a_{mk} with $\mathbf{a}_k = [a_{1k},...,a_{Mk}]^T\in\mathbb{C}^{M\times 1}$ to obtain $\hat{s}_k = \sum_{m=1}^{M}a_{mk}^*\check{s}_{mk}$ as (30) at the top of the next page, in which DE$_k$ is the desired signal, BU$_k$ is the beamforming gain uncertainty, UI$_{kk'}$ is the inter-user interference, EMI$_k$ and NS$_k$ are the respective EMI and noise.

$$\nabla_{\mathbf{u}_{\omega_k}} \mathrm{tr}(\mathbf{Q}_{mk}) \quad = 2A^2 \tau_p p_p \mathrm{tr}\left(\boldsymbol{\Psi}_{mk}^{-1}\boldsymbol{\Delta}_{mk}\boldsymbol{\Pi}_{mk} + \boldsymbol{\Delta}_{mk}\boldsymbol{\Psi}_{mk}^{-1}\boldsymbol{\Pi}_{mk}\right)\Re\mathfrak{E}\left\{\mathrm{diag}\left(\bar{\mathbf{R}}\boldsymbol{\Theta}_{\omega_k}^*\mathbf{R}^T\theta_{\omega_k}^T\right)\right\}$$
$$- 2A^2\tau_p^2 p_p^2 \sum_{k'\in\mathcal{P}_k\cap\mathcal{W}_k} \mathrm{tr}\left(\boldsymbol{\Psi}_{mk}^{-1}\boldsymbol{\Delta}_{mk}^2\boldsymbol{\Psi}_{mk}^{-1}\boldsymbol{\Pi}_{mk'}\right)\Re\mathfrak{E}\left\{\mathrm{diag}\left(\bar{\mathbf{R}}\boldsymbol{\Theta}_{\omega_{k'}}^*\mathbf{R}^T\theta_{\omega_{k'}}^T\right)\right\} \tag{28}$$
$$- 2A^2\tau_p p_p \beta_m \sigma_{\omega_k}^2 \mathrm{tr}\left(\boldsymbol{\Psi}_{mk}^{-1}\boldsymbol{\Delta}_{mk}^2\boldsymbol{\Psi}_{mk}^{-1}\mathbf{R}_{m,r}\right)\Re\mathfrak{E}\left\{\mathrm{diag}\left(\bar{\mathbf{R}}\boldsymbol{\Theta}_{\omega_k}^*\mathbf{R}^T\theta_{\omega_k}^T\right)\right\}.$$

$$\hat{s}_k \quad = \sum_{m=1}^{M} a_{mk}^* \hat{\mathbf{g}}_{mk}^H\left(\sqrt{p_u}\sum_{k=1}^{K}\mathbf{g}_{mk}\sqrt{\eta_k}s_k + \mathbf{g}_m\bar{\boldsymbol{\Theta}}_r\boldsymbol{\Theta}_r\mathbf{n}_r + \mathbf{g}_m\bar{\boldsymbol{\Theta}}_t\boldsymbol{\Theta}_t\mathbf{n}_t + \mathbf{w}_m\right)$$
$$= \underbrace{\sqrt{p_u\eta_k}\sum_{m=1}^{M}a_{mk}^*\mathbb{E}\left\{\hat{\mathbf{g}}_{mk}^H\mathbf{g}_{mk}\right\}s_k}_{\mathrm{DS}_k} + \underbrace{\sqrt{p_u\eta_k}\sum_{m=1}^{M}a_{mk}^*\left(\hat{\mathbf{g}}_{mk}^H\mathbf{g}_{mk} - \mathbb{E}\left\{\hat{\mathbf{g}}_{mk}^H\mathbf{g}_{mk}\right\}\right)s_k}_{\mathrm{BU}_k}$$
$$+ \sum_{k'\neq k}^{K}\underbrace{\sqrt{p_u}\sum_{m=1}^{M}\sqrt{\eta_{k'}}a_{mk}^*\hat{\mathbf{g}}_{mk}^H\mathbf{g}_{mk'}s_{k'}}_{\mathrm{UI}_{kk'}} + \underbrace{\sum_{m=1}^{M}a_{mk}^*\hat{\mathbf{g}}_{mk}^H\mathbf{g}_m\bar{\boldsymbol{\Theta}}_r\boldsymbol{\Theta}_r\mathbf{n}_r + \sum_{m=1}^{M}a_{mk}^*\hat{\mathbf{g}}_{mk}^H\mathbf{g}_m\bar{\boldsymbol{\Theta}}_t\boldsymbol{\Theta}_t\mathbf{n}_t}_{\mathrm{EMI}_k} + \underbrace{\sum_{m=1}^{M}a_{mk}^*\hat{\mathbf{g}}_{mk}^H\mathbf{w}_m}_{\mathrm{NS}_k}. \tag{30}$$

$$\mathrm{SINR}_{\mathrm{u},k} \quad = \frac{\mathbb{E}\{|\mathrm{DS}_k|^2\}}{\mathbb{E}\{|\mathrm{BU}_k|^2\} + \sum_{k'\neq k}^{K}\mathbb{E}\{|\mathrm{UI}_{kk'}|^2\} + \mathbb{E}\{|\mathrm{EMI}_k|^2\} + \mathbb{E}\{|\mathrm{NS}_k|^2\}}$$
$$= \frac{p_u\eta_k\left|\mathbf{a}_k^H\mathbf{b}_k\right|^2}{\sum_{k'\in\mathcal{P}_k}p_u\eta_{k'}\mathbf{a}_k^H\boldsymbol{\Omega}_{kk'}\mathbf{a}_k + \sum_{k'=1}^{K}p_u\eta_{k'}\mathbf{a}_k^H\left(\boldsymbol{\Upsilon}_{kk'} + \bar{\boldsymbol{\Upsilon}}_{kk'}\right)\mathbf{a}_k - p_u\eta_k\left|\mathbf{a}_k^H\mathbf{b}_k\right|^2 + \sigma_t^2\mathbf{a}_k^H\boldsymbol{\Gamma}_{t,k}\mathbf{a}_k + \sigma_r^2\mathbf{a}_k^H\boldsymbol{\Gamma}_{r,k}\mathbf{a}_k + \sigma^2\mathbf{a}_k^H\boldsymbol{\Lambda}_k\mathbf{a}_k}. \tag{32}$$

B. Performance Analysis and Closed-form SE Derivations

The use-and-then-forget (UatF) bound [12], [47] is utilized to determine the uplink SE lower bound. Based on (30), the uplink SE of the k-th user is expressed as

$$\mathrm{SE}_{\mathrm{u},k} = \frac{\tau_c - \tau_p}{\tau_c}\log_2\left(1 + \mathrm{SINR}_{\mathrm{u},k}\right), \tag{31}$$

where the effective signal-to-interference-plus-noise ratio (SINR) is denoted by $\mathrm{SINR}_{\mathrm{u},k}$, and its closed-form expression is given by (32) at the top of this page.

Since the LSFD receiver introduced in [7], [47] can maximize the k-th user's effective SINR, the corresponding weight vector $\mathbf{a}_k \in \mathbb{C}^{M\times 1}$ can be given by

$$\mathbf{a}_k = \left[\sum_{k'\in\mathcal{P}_k}p_u\eta_{k'}\boldsymbol{\Omega}_{kk'} + \sum_{k'=1}^{K}p_u\eta_{k'}\left(\boldsymbol{\Upsilon}_{kk'} + \bar{\boldsymbol{\Upsilon}}_{kk'}\right)\right.$$
$$\left. - p_u\eta_k\mathbf{b}_k\mathbf{b}_k^H + \sigma_t^2\boldsymbol{\Gamma}_{t,k} + \sigma_r^2\boldsymbol{\Gamma}_{r,k} + \sigma^2\boldsymbol{\Lambda}_k\right]^{-1}\mathbf{b}_k. \tag{33}$$

The CPU can optimize the weight vector for the uplink SE maximization. Note that the LSFD receiver achieves the maximum SE with high complexity. The conventional matched filter (MF) receiver in [2], [12] can be utilized for low-complexity transmission by using $\mathbf{a}_k = [1/M, 1/M, ..., 1/M]^T$.

Proof: Please refer to Appendix B.

C. Uplink Power Control

Uplink fractional power control is introduced to reduce the near-far effects in the EMI-aware and phase error-aware environment [13], [48]. The k-th user's uplink power control coefficient, depending on its corresponding large-scale fading coefficients, is formulated as

$$\eta_k = \frac{K \cdot \sum_{m=1}^{M}\mathrm{tr}(\boldsymbol{\Delta}_{mk})}{\sum_{m=1}^{M}\sum_{k'=1}^{K}\mathrm{tr}(\boldsymbol{\Delta}_{mk'})}, \quad \forall k. \tag{34}$$

As a summary of the derivations in this section, note that we can use (31)- (34) to determine the uplink SE performance.

V. DOWNLINK DATA TRANSMISSION AND CLOSED-FORM SE EXPRESSIONS

We derive novel closed-form downlink SE expressions and utilize fractional power control to investigate the downlink performance of the proposed STAR-RIS-assisted cell-free massive MIMO system suffering from EMI and phase errors.

A. Downlink Data Transmission

The precoding vector $\mathbf{f}_{mk} \in \mathbb{C}^{N\times 1}$, $\forall m$, $\forall k$ is utilized to assist the broadcast channel of the downlink data transmission [16]. Since the system is operated under TDD mode, the channel reciprocity characteristic can regard the uplink channel transpose as the downlink channel [13], [39]. Therefore, the transmitted signal by the m-th AP can be obtained as

$$\mathbf{x}_m = \sqrt{p_d}\sum_{k=1}^{K}\mathbf{f}_{mk}\sqrt{\eta_{mk}}q_k, \tag{35}$$

where p_d is the downlink transmit power, $q_k \sim \mathcal{CN}(0,1)$ is the signal transmitted to the k-th user, η_{mk} denotes downlink power control coefficients satisfying $\mathbb{E}\{|\mathbf{x}_m|^2\} \leq p_d$. This work applies conjugate beamforming, that is, $\mathbf{f}_{mk} = \hat{\mathbf{g}}_{mk}^*$. With the assistance of (12), (36) at the top of the next page expresses the received

$$r_k = \sum_{m=1}^{M} \mathbf{g}_{mk}^T \mathbf{x}_m + (\bar{\boldsymbol{\Theta}}_{\omega_k} \boldsymbol{\Theta}_{\omega_k} \mathbf{g}_k)^T \mathbf{n}_r + z_k = \sum_{m=1}^{M} \sum_{k'=1}^{K} \sqrt{\rho_d} \mathbf{g}_{mk}^T \hat{\mathbf{g}}_{mk'}^* \sqrt{\eta_{mk'}} q_k + (\bar{\boldsymbol{\Theta}}_{\omega_k} \boldsymbol{\Theta}_{\omega_k} \mathbf{g}_k)^T \mathbf{n}_r + z_k$$

$$= \underbrace{\sqrt{p_d} \sum_{m=1}^{M} \mathbb{E}\{\mathbf{g}_{mk}^T \hat{\mathbf{g}}_{mk}^*\} \sqrt{\eta_{mk}} q_k}_{\text{DS}_k} + \underbrace{\sqrt{p_d} \sum_{m=1}^{M} \left(\mathbf{g}_{mk}^T \hat{\mathbf{g}}_{mk}^* - \mathbb{E}\{\mathbf{g}_{mk}^T \hat{\mathbf{g}}_{mk}^*\}\right) \sqrt{\eta_{mk}} q_k}_{\text{BU}_k} + \sum_{k' \neq k} \underbrace{\sqrt{\rho_d} \sum_{m=1}^{M} \mathbf{g}_{mk}^T \hat{\mathbf{g}}_{mk'}^* \sqrt{\eta_{mk'}} q_k}_{\text{UI}_{kk'}} + \underbrace{(\bar{\boldsymbol{\Theta}}_{\omega_k} \boldsymbol{\Theta}_{\omega_k} \mathbf{g}_k)^T \mathbf{n}_r}_{\text{EMI}_k} + \underbrace{z_k}_{\text{NS}_k},$$

$$(36)$$

$$\text{SINR}_{\text{d},k} = \frac{p_d \left| \sum_{m=1}^{M} \sqrt{\eta_{mk}} \mathbb{E}\{\mathbf{g}_{mk}^T \hat{\mathbf{g}}_{mk}^*\} \right|^2}{p_d \sum_{k'=1}^{K} \mathbb{E}\left\{ \left| \sum_{m=1}^{M} \sqrt{\eta_{mk'}} \mathbf{g}_{mk}^T \hat{\mathbf{g}}_{mk'}^* \right|^2 \right\} - p_d \left| \sum_{m=1}^{M} \sqrt{\eta_{mk}} \mathbb{E}\{\mathbf{g}_{mk}^T \hat{\mathbf{g}}_{mk}^*\} \right|^2 + \mathbb{E}\left\{ \left| (\bar{\boldsymbol{\Theta}}_{\omega_k} \boldsymbol{\Theta}_{\omega_k} \mathbf{g}_k)^T \mathbf{n}_r \right|^2 \right\} + \sigma^2}$$

$$= \frac{p_d \left| \mathbf{c}_k^H \mathbf{b}_k \right|^2}{\sum_{k' \in \mathcal{P}_k} p_d \mathbf{c}_{k'}^H \boldsymbol{\Omega}_{k'k} \mathbf{c}_{k'} + \sum_{k'=1}^{K} p_d \mathbf{c}_{k'}^H \left(\boldsymbol{\Upsilon}_{k'k} + \bar{\boldsymbol{\Upsilon}}_{k'k}\right) \mathbf{c}_{k'} - p_d \left| \mathbf{c}_k^H \mathbf{b}_k \right|^2 + \beta_k \sigma_r^2 \text{tr}(\mathbf{T}_{\omega_k}) + \sigma^2}. \quad (39)$$

signal at the k-th user where $\mathbf{n}_r \sim \mathcal{CN}(0, A\sigma_r^2 \mathbf{R})$ denotes the EMI from the reflection area, $z_k \sim \mathcal{CN}(0, \sigma^2)$ represents the receiver noise at the k-th user.

B. Performance Analysis and Closed-form SE Derivations

Based on (36), we can lower bound the downlink SE of the k-th user and obtain it by [6], [12]

$$\text{SE}_{\text{d},k} = \frac{\tau_c - \tau_p}{\tau_c} \log_2\left(1 + \text{SINR}_{\text{d},k}\right). \quad (37)$$

We omit the proof procedure since the proof is similar to Appendix B. Meanwhile, the EMI term is given by

$$\mathbb{E}\left\{ \left| (\bar{\boldsymbol{\Theta}}_{\omega_k} \boldsymbol{\Theta}_{\omega_k} \mathbf{g}_k)^T \mathbf{n}_r \right|^2 \right\} = \mathbb{E}\left\{ (\bar{\boldsymbol{\Theta}}_{\omega_k} \boldsymbol{\Theta}_{\omega_k} \mathbf{g}_k)^T \mathbf{n}_r \mathbf{n}_r^H (\bar{\boldsymbol{\Theta}}_{\omega_k} \boldsymbol{\Theta}_{\omega_k} \mathbf{g}_k)^* \right\}$$
$$= \beta_k \sigma_r^2 \text{tr}(\mathbf{T}_{\omega_k}). \quad (38)$$

Then, with the assistance of $\mathbf{c}_k = [\sqrt{\eta_{1k}}, \sqrt{\eta_{2k}}, ..., \sqrt{\eta_{Mk}}]^T \in \mathbb{C}^{M \times 1}$, $\forall k$, (39) at the top of this page shows the closed-form expression of $\text{SINR}_{\text{d},k}$.

C. Downlink Power Control

According to [16], [22], [48], we introduce the fractional power control to meet the downlink power constraint. This work assumes that $\mathbb{E}\{|\mathbf{x}_m|^2\} = p_d$, and the downlink power control coefficients can be obtained as

$$\eta_{mk} = \left(\sum_{k'=1}^{K} \text{tr}(\mathbf{Q}_{mk'}) \right)^{-1}, \forall k, \forall m. \quad (40)$$

As a summary of the derivations in this section, we can utilise (37)-(40) to determine the downlink SE performance.

VI. NUMERICAL RESULTS AND DISCUSSIONS

This section presents numerical results, that demonstrate the impact of EMI and phase errors on the STAR-RIS-assisted cell-free massive MIMO system. These results provide performance limits and system design guidelines. We also introduce the innovative use of the projected GD algorithm, which optimizes the STAR-RIS coefficient matrix to improve system performance. Particularly, (14) and (15) allow us to determine the channel estimation NMSE by applying the projected GD

algorithm with (17)-(18) to optimize (16). (31)- (34) determine the uplink SE performance and (37)-(40) determine the downlink SE performance. The numerical results include Monte Carlo (MC) simulations and closed-form analytical results. The analytical results quantify a mathematical approximation of the average performance over the channel realizations to indicate how design variables affect performance visually.

A. Parameter Setup

In the results, a two-dimensional coordinate system similar to [5], [49] is utilized, and all coordinates are in meters. STAR-RIS is located at $(x^{\text{STAR-RIS}}, y^{\text{STAR-RIS}}) = (500, 100)$, APs are randomly distributed around the origin with $x^{\text{AP}}, y^{\text{AP}} \in [-100, 100]$. Users in the reflection area are located with $x^{\text{user}} \in [400, 600]$ and $y^{\text{user}} \in [0, 100)$, while users in the transmission area are distributed with $x^{\text{user}} \in [450, 550]$ and $y^{\text{user}} \in (100, 150]$. The AP, user and RIS heights are 15m, 1.65m, and 30m [6]. We also apply the path loss model in [2], [22] and follow the relevant settings to express the large-scale fading coefficients as $\beta_x = \text{PL}_x \cdot z_x$ ($x = mk, m, k$). PL_x is the three-slope path loss, z_x is the log-normal shadowing. Unless mentioned, the uplink transmission applies LSFD receiver cooperation, $p_p = p_u = 20$ dBm, $p_d = 23$ dBm, $\sigma^2 = -91$ dBm, and $d_h = d_v = \lambda/4$ for the STAR-RIS elements. Moreover, the AP spatial correlation model follows the exponential correlation model introduced in [13], [50], $f_c = 1.9$ GHz is the carrier frequency, the coherence interval length is $\tau_c = 200$ with the bandwidth $B = 20$ MHz, $\tau_p = 4$ is applied for channel estimation [7]. For the projected GD algorithm, we set the maximum number of iterations IterMax= 100, the initial step size $\mu = 1$ and tolerance $\epsilon = 10^{-6}$ until stated [43].

B. Channel Estimation Accuracy

Channel estimation NMSE versus p_p is displayed in Fig. 2. In this work, the equal STAR-RIS coefficient matrix follows $u_l^\omega = 1/\sqrt{2}$, $\varphi_l^r = \pi/4$, $\varphi_l^t = \varphi_l^r + \pi/2$, $\forall l$. The conventional MMSE scheme with an equal STAR-RIS coefficient matrix without EMI or phase errors is considered as the baseline scenario [7], [16]. The closed-form analytical results calculated
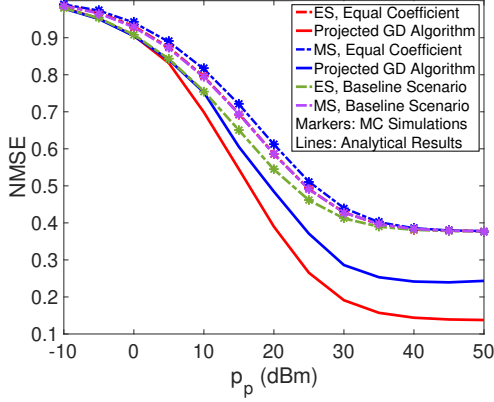
Fig. 2. NMSE vs p_p with $M = 20$, $N = 4$, $K = 12$, $K_t = K_r = 6$, $L = 16$, $\rho = 20$ dB, $d = \lambda/4$ (MC Simulations and Analytical Results).

Fig. 5. Average SE per user vs the number of users K with $M = 20$, $N = 4$, $K_t = K_r$, $d = \lambda/4$ (Analytical Results).

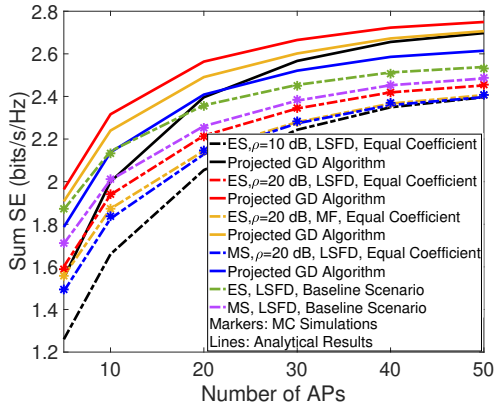
Fig. 3. Sum SE vs the number of APs M with $N = 4$, $K = 12$, $K_t = K_r = 6$, $L = 16$, $d = \lambda/4$ (MC Simulations and Analytical Results).

Fig. 6. Sum SE vs the number of STAR-RIS elements L with $M = 20$, $N = 4$, $K = 12$, $K_t = K_r = 6$ (Analytical Results).

flexibility of the STAR-RIS coefficient matrix design. On the other hand, the proposed projected GD algorithm provides the best performance, significantly increasing estimation accuracy and decreasing NMSE. Our simulations also reveal that the convergence speed of the proposed projected GD algorithm increases with a larger step size, and the random initialization of the STAR-RIS coefficients can affect the convergence speed, agreeing with [40]. When $p_p = 20$ dBm and IterMax= 1000, $\mu = 1$ takes around 100 iterations, $\mu = 0.5$ takes around 200 iterations to converge. Moreover, random initial phase shifts, $\varphi_l^r < \pi$ with $\mu = 1$, take around an average of 300 iterations to converge, while the steady-state NMSE is unaffected.

C. Effects of the Number of APs and Antennas Per AP

Fig. 3 and Fig. 4 represent the sum SE as functions of the number of APs and antennas per AP, respectively, where the sum SE is formulated as $\text{SE}_{\text{sum}} = \frac{1}{2} \sum_{k=1}^{K} (\text{SE}_{\text{u},k} + \text{SE}_{\text{d},k})$. The closed-form analytical results based on (31)- (34) and (37)- (40) can match the numerical results delivered by Monte Carlo simulations closely. It shows that increasing APs and antennas per AP can enhance the sum SE, especially with severe EMI. However, the growth of performance gains will be diminished with the increasing number of APs and antennas per AP. This is because the introduction of increased spatial freedom
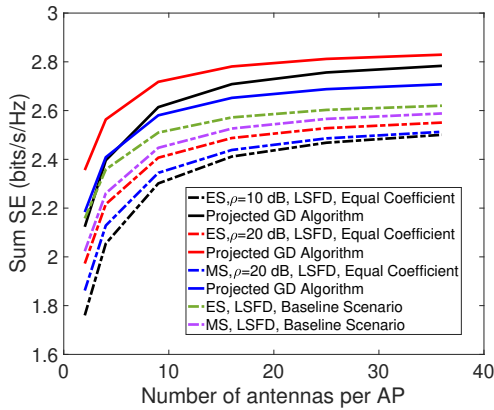

Fig. 4. Sum SE vs the number of antennas per AP N with $M = 20$, $K = 12$, $K_t = K_r = 6$, $L = 16$, $d = \lambda/4$ (Analytical Results).

by (5), (6), (14) and (15) match the performance delivered by Monte Carlo simulations closely. Note that $\tau_p = 4 < K$ causes pilot contamination. The joint effect of EMI and phase errors also reduces the channel estimation accuracy. In this case, a non-zero error floor occurs even when p_p is increased. In addition, as a special case of ES protocol, the MS protocol experiences a worse NMSE since the MS protocol contains restricted amplitude coefficients as binary values, lessening the
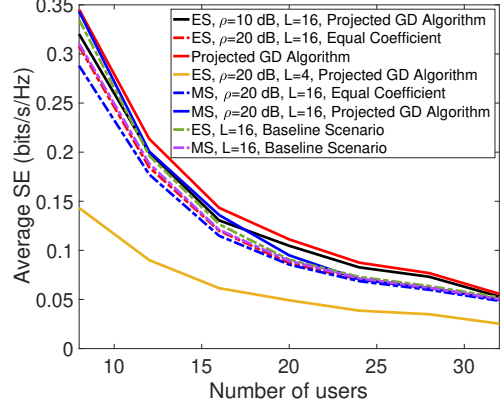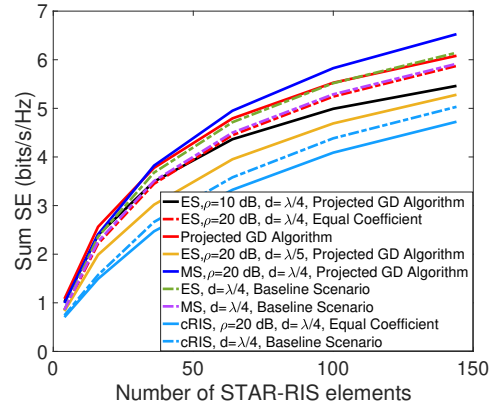
cannot make up for the significantly increasing inter-user interference, EMI and network overhead. Fig. 3 reveals that for the ES protocol, the sum SE with the proposed projected GD algorithm can introduce a larger 22% to 12%-likely SE than that with the equal coefficient matrix, decreasing growth trend with the increasing number of APs. Moreover, the sum SE with LSFD can introduce a larger 3%-likely SE than that with MF. The harsh propagation conditions bring up the limited performance gain. Similarly, Fig. 4 indicates that the sum SE with the proposed projected GD algorithm introduces a larger 20% to 10%-likely SE than that with the equal coefficient matrix, experiencing a decreased growth trend. Meanwhile, the proposed system with the projected GD algorithm can outperform the baseline scenarios. Similar to Fig. 2, the sum SE of the MS protocol performs worse than that of the ES protocol. However, more APs and antennas per AP cannot fully release their benefits under harsh propagation conditions. Thus, the number of APs and antennas per AP must be appropriately raised to meet the required system performance.

D. Effects of the Number of users

The average SE per user, determined by $\text{SE}_{\text{ave}} = \text{SE}_{\text{sum}}/K$, is displayed in Fig. 5 as a function of the number of users with different STAR-RIS elements. The results reveal that increasing the number of users decreases the average performance since more users increase inter-user interference and introduce more severe pilot contamination. Note that increasing the number of STAR-RIS elements can compensate for the decrease in performance caused by increasing users since more STAR-RIS elements can introduce more reflected energy and transmitted energy in their respective areas. Moreover, the proposed projected GD algorithm can help to improve the average SE per user with EMI and phase errors. However, a topic derived from this is scalable implementation since the number of users might be extremely large, which introduces high computational complexity and processing overhead [9], [20]. Thus, it is crucial to introduce advanced signal-processing methods to eliminate pilot contamination and inter-user interference. Moreover, a future topic might be introducing STAR-RISs in user-centric cell-free massive MIMO where fewer APs serve each user to achieve low-complexity computational feasibility.

E. Effects of the Number of STAR-RIS Elements

Fig. 6 indicates the sum SE as a function of the number of STAR-RIS elements. We can find that increasing the number of STAR-RIS elements could significantly enhance the system performance with a gradually decreasing growth trend. Moreover, we can find that smaller inter-element distance introduces higher spatial correlation to decrease the system performance. A remarkable insight is that more STAR-RIS elements increase the performance of the MS protocol, surpassing that of the ES protocol under harsh propagation conditions. This is because more STAR-RIS elements will introduce more severe EMI and phase errors to degrade the system performance. The MS protocol might introduce higher energy in the area where users are close to the APs to maintain performance. To further show the benefits of STAR-RIS deployment, we present a benchmark scenario with a conventional transmitting-only RIS and a reflecting-only RIS positioned next to each other at the exact STAR-RIS location. For fairness, each conventional RIS (cRIS) is assumed to have $L/2$ elements [1]. It shows that the proposed STAR-RIS-assisted system can achieve a 25%-likely SE improvement than that with cRISs, which motivates the deployment of STAR-RISs in cell-free massive MIMO systems. Appropriately increasing the number of STAR-RIS elements can improve system performance with EMI and phase errors. Meanwhile, EMI elimination and phase error compensation methods should be introduced to enhance the benefits of deploying more STAR-RIS elements.

VII. Conclusion

STAR-RIS-assisted cell-free massive MIMO represents a sustainable and attractive architecture that leverages their combined advantages. To our knowledge, this work is the first to analyze the performance of spatially correlated STAR-RIS-assisted cell-free massive MIMO systems, taking into account the impacts of EMI and phase errors while conducting SE performance analysis. We introduced the projected GD algorithm for designing the STAR-RIS coefficient matrix, aimed at minimizing the NMSE. We derived the closed-form expressions of the uplink and downlink SE with respective uplink LSFD decoding and downlink conjugate beamforming for performance evaluation. The results reveal that EMI and phase errors cause non-negligible degradation in channel estimation accuracy and sum SE. Our proposed projected GD algorithm can improve estimation accuracy and introduce a 10% ∼ 20%-likely SE improvement. Increasing APs/AP antennas and STAR-RIS elements can also reduce performance degradation. However, severe EMI could mitigate the advantages of increasing STAR-RIS elements. More users might introduce severe inter-user interference and pilot contamination to reduce the average SE per user. Distinct from the conventional insight that the ES protocol outperforms the MS protocol with increasing APs/AP antennas, the MS protocol can outperform the ES protocol under harsh propagation conditions with increasing STAR-RIS elements. Moreover, STAR-RIS achieves a larger 25%-likely SE than conventional RISs, underscoring the necessity of deploying STAR-RISs in cell-free massive MIMO. Inspired by these results, our future work will focus on scalable implementation, advanced channel estimation schemes, inter-user interference and EMI mitigation methods to sufficiently realize the advantages of deploying STAR-RISs in the cell-free massive MIMO to serve more users.

Appendix A
Proof of Complex Gradients

This appendix delivers the derivations of complex gradients in (23) regarding $\boldsymbol{\theta}$ and $\mathbf{u}$. First, we study the derivation of $\nabla_{\boldsymbol{\theta}_{\omega_k}}\text{NMSE}_{mk}(\boldsymbol{\theta}, \mathbf{u})$. When considering $\text{tr}(\mathbf{T}_{\omega_k})$, we can obtain

$$
\begin{aligned}
d\text{tr}(\mathbf{T}_{\omega_k}) &= \text{tr}\Big(d(A^2\mathbf{R}^{1/2}\bar{\boldsymbol{\Theta}}_{\omega_k}\boldsymbol{\Theta}_{\omega_k}\mathbf{R}\boldsymbol{\Theta}_{\omega_k}^H\bar{\boldsymbol{\Theta}}_{\omega_k}^H\mathbf{R}^{1/2})\Big) \\
&= A^2\text{tr}\Big(\mathbf{u}_{\omega_k}\mathbf{R}\boldsymbol{\Theta}_{\omega_k}^H\bar{\mathbf{R}}d\theta_{\omega_k} + \big(\bar{\mathbf{R}}\boldsymbol{\Theta}_{\omega_k}\mathbf{R}\mathbf{u}_{\omega_k}^H\big)^T d\theta_{\omega_k}^*\Big),
\end{aligned}
\tag{41}
$$

$$d(\mathbf{Q}_{mk}) = d(\tau_p p_p \mathbf{\Delta}_{mk} \mathbf{\Psi}_{mk}^{-1} \mathbf{\Delta}_{mk}) = \tau_p p_p \left(d(\mathbf{\Delta}_{mk}) \mathbf{\Psi}_{mk}^{-1} \mathbf{\Delta}_{mk} + \mathbf{\Delta}_{mk} d(\mathbf{\Psi}_{mk}^{-1}) \mathbf{\Delta}_{mk} + \mathbf{\Delta}_{mk} \mathbf{\Psi}_{mk}^{-1} d(\mathbf{\Delta}_{mk}) \right)$$
$$= \tau_p p_p \left(d(\mathbf{\Delta}_{mk}) \mathbf{\Psi}_{mk}^{-1} \mathbf{\Delta}_{mk} - \mathbf{\Delta}_{mk} \mathbf{\Psi}_{mk}^{-1} d(\mathbf{\Psi}_{mk}) \mathbf{\Psi}_{mk}^{-1} \mathbf{\Delta}_{mk} + \mathbf{\Delta}_{mk} \mathbf{\Psi}_{mk}^{-1} d(\mathbf{\Delta}_{mk}) \right), \tag{47}$$

$$d(\mathrm{tr}(\mathbf{Q}_{mk})) = \mathrm{tr}(d(\mathbf{Q}_{mk})) = \mathrm{tr}\left[\tau_p p_p \left(d(\mathbf{\Delta}_{mk}) \mathbf{\Psi}_{mk}^{-1} \mathbf{\Delta}_{mk} - \mathbf{\Delta}_{mk} \mathbf{\Psi}_{mk}^{-1} d(\mathbf{\Psi}_{mk}) \mathbf{\Psi}_{mk}^{-1} \mathbf{\Delta}_{mk} + \mathbf{\Delta}_{mk} \mathbf{\Psi}_{mk}^{-1} d(\mathbf{\Delta}_{mk}) \right) \right]$$
$$= \tau_p p_p \mathrm{tr}\Big(\mathbf{\Pi}_{mk} d\mathrm{tr}(\mathbf{T}_{\omega_k}) \mathbf{\Psi}_{mk}^{-1} \mathbf{\Delta}_{mk} + \mathbf{\Delta}_{mk} \mathbf{\Psi}_{mk}^{-1} \mathbf{\Pi}_{mk} d\mathrm{tr}(\mathbf{T}_{\omega_k})$$
$$- \mathbf{\Delta}_{mk} \mathbf{\Psi}_{mk}^{-1} \Big(\tau_p p_p \sum_{k' \in \mathcal{P}_k} \mathbf{\Pi}_{mk'} d\mathrm{tr}(\mathbf{T}_{\omega_{k'}}) + \beta_m \sigma_r^2 \mathbf{R}_{m,r} d\mathrm{tr}(\mathbf{T}_r) + \beta_m \sigma_t^2 \mathbf{R}_{m,r} d\mathrm{tr}(\mathbf{T}_t) \Big) \mathbf{\Psi}_{mk}^{-1} \mathbf{\Delta}_{mk} \Big)$$
$$= \tau_p p_p \mathrm{tr}\Big(\mathbf{\Psi}_{mk}^{-1} \mathbf{\Delta}_{mk} \mathbf{\Pi}_{mk} + \mathbf{\Delta}_{mk} \mathbf{\Psi}_{mk}^{-1} \mathbf{\Pi}_{mk} \Big) d\mathrm{tr}(\mathbf{T}_{\omega_k}) - \tau_p^2 p_p^2 \sum_{k' \in \mathcal{P}_k} \mathrm{tr}\Big(\mathbf{\Psi}_{mk}^{-1} \mathbf{\Delta}_{mk}^2 \mathbf{\Psi}_{mk}^{-1} \mathbf{\Pi}_{mk'} \Big) d\mathrm{tr}(\mathbf{T}_{\omega_{k'}})$$
$$- \tau_p p_p \beta_m \sigma_r^2 \mathrm{tr}\Big(\mathbf{\Psi}_{mk}^{-1} \mathbf{\Delta}_{mk}^2 \mathbf{\Psi}_{mk}^{-1} \mathbf{R}_{m,r} \Big) d\mathrm{tr}(\mathbf{T}_r) - \tau_p p_p \beta_m \sigma_t^2 \mathrm{tr}\Big(\mathbf{\Psi}_{mk}^{-1} \mathbf{\Delta}_{mk}^2 \mathbf{\Psi}_{mk}^{-1} \mathbf{R}_{m,r} \Big) d\mathrm{tr}(\mathbf{T}_t), \tag{48}$$

since $\boldsymbol{\theta}_\omega$ is a diagonal matrix, then so must $d\boldsymbol{\theta}_\omega$. With the help of [45], we can obtain

$$\nabla_{\boldsymbol{\theta}_{\omega_k}} \mathrm{tr}(\mathbf{T}_{\omega_k}) = A^2 \Big(\mathbf{u}_{\omega_k} \mathbf{R} \mathbf{\Theta}_{\omega_k}^H \bar{\mathbf{R}} \Big)^T \circ \mathbf{I} = A^2 \mathrm{diag}\Big(\bar{\mathbf{R}} \mathbf{\Theta}_{\omega_k}^* \mathbf{R}^T \mathbf{u}_{\omega_k}^T \Big). \tag{42}$$

Based on $\mathbf{\Delta}_{mk}$ in (5) and $\mathbf{\Psi}_{mk}$ in (13), we can derive the differentials $d(\mathbf{\Delta}_{mk})$ and $d((\mathbf{\Psi}_{mk})^{-1})$ as follows. With respect to $d(\mathbf{\Delta}_{mk})$, we can obtain [45], [46]

$$d(\mathbf{\Delta}_{mk}) = d\big(\beta_m \beta_k \mathrm{tr}(\mathbf{T}_{\omega_k}) \mathbf{R}_{m,r} \big) = \mathbf{\Pi}_{mk} d\mathrm{tr}(\mathbf{T}_{\omega_k}), \tag{43}$$

where $\mathbf{\Pi}_{mk} = \beta_m \beta_k \mathbf{R}_{m,r}$. By applying (41)-(42), we can have

$$\nabla_{\boldsymbol{\theta}_{\omega_k}} \mathrm{tr}(\mathbf{\Delta}_{mk}) = A^2 \beta_m \beta_k \mathrm{tr}\big(\mathbf{R}_{m,r} \big) \mathrm{diag}\big(\bar{\mathbf{R}} \mathbf{\Theta}_{\omega_k}^* \mathbf{R}^T \mathbf{u}_{\omega_k}^T \big). \tag{44}$$

Referring to [5], [51], we can derive $d(\mathbf{\Psi}_{mk}^{-1})$ as

$$d(\mathbf{\Psi}_{mk}^{-1}) = -\mathbf{\Psi}_{mk}^{-1} d(\mathbf{\Psi}_{mk}) \mathbf{\Psi}_{mk}^{-1}, \tag{45}$$

where $d(\mathbf{\Psi}_{mk})$ can be obtained by

$$d(\mathbf{\Psi}_{mk}) = d\Big(\tau_p p_p \sum_{k' \in \mathcal{P}_k} \mathbf{\Delta}_{mk'}$$
$$+ \big(\beta_m \sigma_r^2 \mathrm{tr}(\mathbf{T}_r) + \beta_m \sigma_t^2 \mathrm{tr}(\mathbf{T}_t) \big) \mathbf{R}_{m,r} + \sigma^2 \mathbf{I}_N \Big)$$
$$= \tau_p p_p \sum_{k' \in \mathcal{P}_k} d(\mathbf{\Delta}_{mk'})$$
$$+ \beta_m \sigma_r^2 \mathbf{R}_{m,r} d\mathrm{tr}(\mathbf{T}_r) + \beta_m \sigma_t^2 \mathbf{R}_{m,r} d\mathrm{tr}(\mathbf{T}_t)$$
$$= \tau_p p_p \sum_{k' \in \mathcal{P}_k} \mathbf{\Pi}_{mk'} d\mathrm{tr}(\mathbf{T}_{\omega_{k'}})$$
$$+ \beta_m \sigma_r^2 \mathbf{R}_{m,r} d\mathrm{tr}(\mathbf{T}_r) + \beta_m \sigma_t^2 \mathbf{R}_{m,r} d\mathrm{tr}(\mathbf{T}_t), \tag{46}$$

Then, based on the above differentials, we can obtain $d(\mathbf{Q}_{mk})$ as (47) and the differential of $\mathrm{tr}(\mathbf{Q}_{mk})$ as (48) at the top of this page [5], [51]. Next, we can obtain the derivative $\nabla_{\boldsymbol{\theta}_{\omega_k}} \mathrm{tr}(\mathbf{Q}_{mk})$ in (26). Similarly, we obtain the derivation of $\nabla_{\mathbf{u}_{\omega_k}} \mathrm{NMSE}_{mk}(\boldsymbol{\theta}, \mathbf{u})$ by considering the differential of $\mathrm{tr}(\mathbf{T}_{\omega_k})$ with respect to $\mathbf{u}_{\omega_k}$ as

$$d\mathrm{tr}(\mathbf{T}_{\omega_k}) = \mathrm{tr}\Big(d(A^2 \mathbf{R}^{1/2} \bar{\mathbf{\Theta}}_{\omega_k} \mathbf{\Theta}_{\omega_k} \mathbf{R} \mathbf{\Theta}_{\omega_k}^H \bar{\mathbf{\Theta}}_{\omega_k}^H \mathbf{R}^{1/2}) \Big)$$
$$= A^2 \mathrm{tr}\Big(\boldsymbol{\theta}_{\omega_k} \mathbf{R} \mathbf{\Theta}_{\omega_k}^H \bar{\mathbf{R}} d\mathbf{u}_{\omega_k} + \bar{\mathbf{R}} \mathbf{\Theta}_{\omega_k} \mathbf{R} \boldsymbol{\theta}_{\omega_k}^H d\mathbf{u}_{\omega_k} \Big), \tag{49}$$

since $\mathbf{u}_\omega$ is a real-valued diagonal matrix, then so must $d\mathbf{u}_\omega$. With the assistance of [45], we can calculate

$$\nabla_{\mathbf{u}_{\omega_k}} \mathrm{tr}(\mathbf{T}_{\omega_k}) = A^2 \Big(\boldsymbol{\theta}_{\omega_k} \mathbf{R} \mathbf{\Theta}_{\omega_k}^H \bar{\mathbf{R}} + \bar{\mathbf{R}} \mathbf{\Theta}_{\omega_k} \mathbf{R} \boldsymbol{\theta}_{\omega_k}^H \Big)^T \circ \mathbf{I}$$
$$= 2A^2 \mathfrak{Re}\Big\{ \mathrm{diag}\big(\bar{\mathbf{R}} \mathbf{\Theta}_{\omega_k}^* \mathbf{R}^T \boldsymbol{\theta}_{\omega_k}^T \big) \Big\}. \tag{50}$$

With the differential of $d(\mathbf{\Delta}_{mk})$ introduced in (43), we can obtain the $\nabla_{\mathbf{u}_{\omega_k}} \mathrm{tr}(\mathbf{\Delta}_{mk})$ with the assistance of (49)-(50), as

$$\nabla_{\mathbf{u}_{\omega_k}} \mathrm{tr}(\mathbf{\Delta}_{mk}) = 2A^2 \beta_m \beta_k \mathrm{tr}\big(\mathbf{R}_{m,r} \big) \mathfrak{Re}\Big\{ \mathrm{diag}\big(\bar{\mathbf{R}} \mathbf{\Theta}_{\omega_k}^* \mathbf{R}^T \boldsymbol{\theta}_{\omega_k}^T \big) \Big\}. \tag{51}$$

Similarly, we can easily obtain the derivative process of $\nabla_{\mathbf{u}_{\omega_k}} \mathrm{tr}(\mathbf{Q}_{mk})$ following (48), and the derivative is shown in (28). We omit the details for brevity.

APPENDIX B
DERIVATION OF SE TERM APPROXIMATIONS

We introduce the detailed derivation of every term of $\mathrm{SINR}_{\mathrm{u},k}$ in this appendix [12], [47]. First, the estimate $\hat{\mathbf{g}}_{mk}$ and the estimation error $\tilde{\mathbf{g}}_{mk}$ are uncorrelated based on the properties of MMSE estimation [13], [16]. If users are in the same pilot sequence set, $k' \in \mathcal{P}_k$, $\hat{\mathbf{g}}_{mk'}$ is correlated with $\mathbf{g}_{mk}$.

A. Useful formulas

Inspired by [3], [52], $\mathbb{E}\{|\mathbf{g}_{mk}^H \mathbf{g}_{mk}|^2\}$ can be computed by introducing the normalised vector

$$\mathbf{z} = \frac{\mathbf{g}_{mk}}{\|(\beta_m \mathrm{tr}(\mathbf{R}_{m,r}) \mathbf{R}_{m,t})^{1/2} \bar{\mathbf{\Theta}}_{\omega_k} \mathbf{\Theta}_{\omega_k} \mathbf{g}_k\|}, \tag{52}$$

with $\mathbf{z} \sim \mathcal{CN}\Big(\mathbf{0}, \frac{\mathbf{R}_{m,r}}{\mathrm{tr}(\mathbf{R}_{m,r})} \Big)$. We can decompose $\mathbb{E}\{|\mathbf{g}_{mk}^H \mathbf{g}_{mk}|^2\}$ as

$$\mathbb{E}\{|\mathbf{g}_{mk}^H \mathbf{g}_{mk}|^2\} = \mathbb{E}\Big\{ \|(\beta_m \mathrm{tr}(\mathbf{R}_{m,r}) \mathbf{R}_{m,t})^{1/2} \bar{\mathbf{\Theta}}_{\omega_k} \mathbf{\Theta}_{\omega_k} \mathbf{g}_k\|^4 \|\mathbf{z}\|^4 \Big\}$$
$$= \beta_m^2 \mathrm{tr}(\mathbf{R}_{m,r})^2 \mathbb{E}\Big\{ \|\mathbf{R}_{m,t}^{1/2} \bar{\mathbf{\Theta}}_{\omega_k} \mathbf{\Theta}_{\omega_k} \mathbf{g}_k\|^4 \|\mathbf{z}\|^4 \Big\}$$
$$= \beta_m^2 \beta_k^2 \mathrm{tr}(\mathbf{R}_{m,r})^2 \big(\mathrm{tr}(\mathbf{T}_{\omega_k}^2) + \mathrm{tr}(\mathbf{T}_{\omega_k})^2 \big) \mathbb{E}\{\|\mathbf{z}\|^4\}$$
$$= \beta_m^2 \beta_k^2 \big(\mathrm{tr}(\mathbf{T}_{\omega_k}^2) + \mathrm{tr}(\mathbf{T}_{\omega_k})^2 \big) \big(\mathrm{tr}(\mathbf{R}_{m,r}^2) + \mathrm{tr}(\mathbf{R}_{m,r})^2 \big). \tag{53}$$

With the assistance of (53), we can obtain $\mathbb{E}\{|\mathbf{g}_{mk}^H \mathbf{Z}_{mk}^H \mathbf{g}_{mk}|^2\}$ as (55), $\mathbb{E}\{\mathbf{g}_{mk}^H \mathbf{Z}_{mk}^H \mathbf{g}_{mk} \mathbf{g}_{nk} \mathbf{Z}_{nk}^H \mathbf{g}_{nk}\}$ as (56) and $\mathbb{E}\{|\mathbf{g}_{mk'}^H \mathbf{Z}_{mk}^H \mathbf{g}_{mk}|^2\}$ as (57) at the top of the next page with $\mathbf{Z}_{mk} = \sqrt{\tau_p p_p} \mathbf{\Delta}_{mk} \mathbf{\Psi}_{mk}^{-1}$. Moreover, when $\omega_k = \omega_{k'}$, $\forall k, k'$, we can have

$$\mathbf{T}_{\omega_k} \mathbf{T}_{\omega_{k'}} \triangleq A^4 \mathbf{R}^{1/2} \Big[\bar{\mathbf{R}}_{\omega_k} \mathbf{R} \bar{\mathbf{R}}_{\omega_k} - \big(\bar{\mathbf{R}}_{\omega_k} \mathbf{R} \bar{\mathbf{R}}_{\omega_k} \big) \circ \mathbf{I}_L \Big] \mathbf{R}^{1/2}$$
$$+ A^4 \mathbf{R}^{1/2} \Big[\big(\mathbf{\Theta}_{\omega_k}^H \mathbf{R} \bar{\mathbf{R}}_{\omega_k} \mathbf{R} \mathbf{\Theta}_{\omega_k} \big) \circ \mathbf{I}_L \Big] \mathbf{R}^{1/2}. \tag{54}$$

B. Compute $\mathbb{E}\{|DS_k|^2\}$

First, we can obtain the desired signal as

$$\mathbb{E}\{|DS_k|^2\} = \mathbb{E}\Big\{ \Big| \sqrt{p_u \eta_k} \sum_{m=1}^M a_{mk}^* \mathbb{E}\{\hat{\mathbf{g}}_{mk}^H \mathbf{g}_{mk}\} \Big|^2 \Big\}$$
$$= p_u \eta_k \Big| \sum_{m=1}^M a_{mk}^* \mathbb{E}\{|\hat{\mathbf{g}}_{mk}|^2\} \Big|^2$$
$$= p_u \eta_k \Big| \sum_{m=1}^M a_{mk}^* \mathrm{tr}(\mathbf{Q}_{mk}) \Big|^2$$
$$= p_u \eta_k \big| \mathbf{a}_k^H \mathbf{b}_k \big|^2, \tag{58}$$

with $\mathbf{b}_k = [b_{1k}, ..., b_{Mk}]^T \in \mathbb{C}^{M \times 1}$, $b_{mk} = \mathrm{tr}(\mathbf{Q}_{mk})$, $\forall m$, $\forall k$.

$$\mathbb{E}\left\{|\mathbf{g}_{mk}^H \mathbf{Z}_{mk}^H \mathbf{g}_{mk}|^2\right\} = \beta_m^2 \beta_k^2 \left(\text{tr}(\mathbf{T}_{\omega_k}^2) + \text{tr}(\mathbf{T}_{\omega_k})^2\right)\left(\text{tr}(\mathbf{R}_{m,r}\mathbf{Z}_{mk}^H \mathbf{R}_{m,r}\mathbf{Z}_{mk}) + \text{tr}(\mathbf{R}_{m,r}\mathbf{Z}_{mk}^H)^2\right). \tag{55}$$

$$\mathbb{E}\left\{\mathbf{g}_{mk}^H \mathbf{Z}_{mk}^H \mathbf{g}_{mk}\mathbf{g}_{nk}^H \mathbf{Z}_{nk}\mathbf{g}_{nk}\right\} = \beta_m\beta_n\beta_k^2\text{tr}(\mathbf{R}_{m,r}\mathbf{Z}_{mk}^H)\text{tr}(\mathbf{R}_{n,r}\mathbf{Z}_{nk})\left(\text{tr}(\mathbf{T}_{\omega_k}^2) + \text{tr}(\mathbf{T}_{\omega_k})^2\right). \tag{56}$$

$$\mathbb{E}\left\{|\mathbf{g}_{mk'}^H \mathbf{Z}_{mk}^H \mathbf{g}_{mk}|^2\right\} = \mathbb{E}\left\{|\mathbf{g}_{mk'}^H (\mathbf{Z}_{mk}^H)^{1/2}|^2 |(\mathbf{Z}_{mk}^H)^{1/2}\mathbf{g}_{mk}|^2\right\} = \beta_m^2\beta_{k'}\beta_k\left(\text{tr}(\mathbf{R}_{m,r}\mathbf{Z}_{mk}^H \mathbf{R}_{m,r}\mathbf{Z}_{mk})\text{tr}(\mathbf{T}_{\omega_k})\text{tr}(\mathbf{T}_{\omega_{k'}}) + \text{tr}(\mathbf{R}_{m,r}\mathbf{Z}_{mk}^H)^2\text{tr}(\mathbf{T}_{\omega_k}\mathbf{T}_{\omega_{k'}})\right). \tag{57}$$

$$
\begin{aligned}
T_1 &= \sum_{k'\in\mathcal{P}_k} p_u\eta_{k'}a_{mk}^* a_{mk}^T \left\{
\begin{array}{l}
\tau_p p_p\mathbb{E}\left\{\sum_{k''\in\mathcal{P}_k}\mathbf{g}_{mk''}^H \mathbf{Z}_{mk}^H \mathbf{g}_{mk'}\mathbf{g}_{mk'}^H \mathbf{Z}_{mk}\mathbf{g}_{mk''}\right\} + \mathbb{E}\left\{(\mathbf{g}_m\bar{\boldsymbol{\Theta}}_t\boldsymbol{\Theta}_t\mathbf{N}_t\varphi_k)^H \mathbf{Z}_{mk}^H \mathbf{g}_{mk'}\mathbf{g}_{mk'}^H \mathbf{Z}_{mk}(\mathbf{g}_m\bar{\boldsymbol{\Theta}}_t\boldsymbol{\Theta}_t\mathbf{N}_t\varphi_k)\right\} \\
+\mathbb{E}\left\{(\mathbf{g}_m\bar{\boldsymbol{\Theta}}_r\boldsymbol{\Theta}_r\mathbf{N}_r\varphi_k)^H \mathbf{Z}_{mk}^H \mathbf{g}_{mk'}\mathbf{g}_{mk'}^H \mathbf{Z}_{mk}(\mathbf{g}_m\bar{\boldsymbol{\Theta}}_r\boldsymbol{\Theta}_r\mathbf{N}_r\varphi_k)\right\} + \mathbb{E}\left\{(\mathbf{N}_{m,p}\varphi_k)^H \mathbf{Z}_{mk}^H \mathbf{g}_{mk'}\mathbf{g}_{mk'}^H \mathbf{Z}_{mk}(\mathbf{N}_{m,p}\varphi_k)\right\}
\end{array}
\right\} \\
&= \sum_{k'\in\mathcal{P}_k} p_u\eta_{k'}a_{mk}^* a_{mk}^T \left\{
\begin{array}{l}
\tau_p p_p(\beta_m\beta_{k'})^2\left[\text{tr}(\mathbf{T}_{\omega_{k'}})^2\text{tr}(\mathbf{R}_{m,r}\mathbf{Z}_{mk}^H)^2 + \text{tr}(\mathbf{T}_{\omega_{k'}}^2)\text{tr}(\mathbf{R}_{m,r}\mathbf{Z}_{mk}^H \mathbf{R}_{m,r}\mathbf{Z}_{mk})\right] \\
+\tau_p p_p\sum_{k''\in\mathcal{P}_k}\beta_m^2\beta_{k'}\beta_{k''}\left[\text{tr}(\mathbf{R}_{m,r}\mathbf{Z}_{mk}^H \mathbf{R}_{m,r}\mathbf{Z}_{mk})\text{tr}(\mathbf{T}_{\omega_{k'}})\text{tr}(\mathbf{T}_{\omega_{k''}}) + \text{tr}(\mathbf{R}_{m,r}\mathbf{Z}_{mk}^H)^2\text{tr}(\mathbf{T}_{\omega_{k'}}\mathbf{T}_{\omega_{k''}})\right] \\
+\beta_m^2\beta_{k'}\sigma_t^2\left[\text{tr}(\mathbf{R}_{m,r}\mathbf{Z}_{mk}^H \mathbf{R}_{m,r}\mathbf{Z}_{mk})\text{tr}(\mathbf{T}_{\omega_{k'}})\text{tr}(\mathbf{T}_t) + \text{tr}(\mathbf{R}_{m,r}\mathbf{Z}_{mk}^H)^2\text{tr}(\mathbf{T}_{\omega_{k'}}\mathbf{T}_t)\right] \\
+\beta_m^2\beta_{k'}\sigma_r^2\left[\text{tr}(\mathbf{R}_{m,r}\mathbf{Z}_{mk}^H \mathbf{R}_{m,r}\mathbf{Z}_{mk})\text{tr}(\mathbf{T}_{\omega_{k'}})\text{tr}(\mathbf{T}_r) + \text{tr}(\mathbf{R}_{m,r}\mathbf{Z}_{mk}^H)^2\text{tr}(\mathbf{T}_{\omega_{k'}}\mathbf{T}_r)\right] + \sigma^2\text{tr}\left(\boldsymbol{\Delta}_{mk'}\mathbf{Z}_{mk}\mathbf{Z}_{mk}^H\right)
\end{array}
\right\},
\end{aligned}
\tag{61}
$$

$$
\begin{aligned}
T_2 &= \sum_{k'\in\mathcal{P}_k} p_u\eta_{k'}\sum_{m=1}^M\sum_{n\neq m} a_{mk}^* a_{nk}^T \left\{
\begin{array}{l}
\tau_p p_p\mathbb{E}\left\{\sum_{k''\in\mathcal{P}_k}\mathbf{g}_{mk''}^H \mathbf{Z}_{mk}^H \mathbf{g}_{mk'}\mathbf{g}_{nk'}^H \mathbf{Z}_{nk}\mathbf{g}_{nk''}\right\} + \mathbb{E}\left\{(\mathbf{g}_m\bar{\boldsymbol{\Theta}}_t\boldsymbol{\Theta}_t\mathbf{N}_t\varphi_k)^H \mathbf{Z}_{mk}^H \mathbf{g}_{mk'}\mathbf{g}_{nk'}^H \mathbf{Z}_{nk}(\mathbf{g}_n\bar{\boldsymbol{\Theta}}_t\boldsymbol{\Theta}_t\mathbf{N}_t\varphi_k)\right\} \\
+\mathbb{E}\left\{(\mathbf{g}_m\bar{\boldsymbol{\Theta}}_r\boldsymbol{\Theta}_r\mathbf{N}_r\varphi_k)^H \mathbf{Z}_{mk}^H \mathbf{g}_{mk'}\mathbf{g}_{nk'}^H \mathbf{Z}_{nk}(\mathbf{g}_n\bar{\boldsymbol{\Theta}}_r\boldsymbol{\Theta}_r\mathbf{N}_r\varphi_k)\right\} + \mathbb{E}\left\{(\mathbf{N}_{m,p}\varphi_k)^H \mathbf{Z}_{mk}^H \mathbf{g}_{mk'}\mathbf{g}_{mk'}^H \mathbf{Z}_{nk}(\mathbf{N}_{n,p}\varphi_k)\right\}
\end{array}
\right\} \\
&= \sum_{k'\in\mathcal{P}_k} p_u\eta_{k'}\sum_{m=1}^M\sum_{n\neq m} a_{mk}^* a_{nk}^T \left\{
\begin{array}{l}
\tau_p p_p\beta_m\beta_n\left(\beta_{k'}^2\text{tr}(\mathbf{R}_{m,r}\mathbf{Z}_{mk}^H)\text{tr}(\mathbf{R}_{n,r}\mathbf{Z}_{nk})\text{tr}(\mathbf{T}_{\omega_{k'}})^2 + \sum_{k''\in\mathcal{P}_k}\beta_{k'}\beta_{k''}\text{tr}(\mathbf{R}_{m,r}\mathbf{Z}_{mk}^H)\text{tr}(\mathbf{R}_{n,r}\mathbf{Z}_{nk})\text{tr}(\mathbf{T}_{\omega_{k'}}\mathbf{T}_{\omega_{k''}})\right) \\
+\beta_m\beta_n\beta_{k'}\text{tr}(\mathbf{R}_{m,r}\mathbf{Z}_{mk}^H)\text{tr}(\mathbf{R}_{n,r}\mathbf{Z}_{nk})\left[\sigma_t^2\text{tr}(\mathbf{T}_{\omega_{k'}}\mathbf{T}_t) + \sigma_r^2\text{tr}(\mathbf{T}_{\omega_{k'}}\mathbf{T}_r)\right]
\end{array}
\right\},
\end{aligned}
\tag{62}
$$

C. Compute $\mathbb{E}\{|UI_{kk'}|^2\}$

We first decompose the sum of inter-user interference into

$$\sum_{k'=1}^M \mathbb{E}\left\{|UI_{kk'}|^2\right\} = \sum_{k'\in\mathcal{P}_k}\mathbb{E}\left\{|UI_{kk'}|^2\right\} + \sum_{k'\notin\mathcal{P}_k}\mathbb{E}\left\{|UI_{kk'}|^2\right\}. \tag{59}$$

1) $\sum_{k'\in\mathcal{P}_k}\mathbb{E}\{|UI_{kk'}|^2\}$: The procedure shows that

$$
\begin{aligned}
\sum_{k'\in\mathcal{P}_k}\mathbb{E}\left\{|UI_{kk'}|^2\right\} &= \sum_{k'\in\mathcal{P}_k} p_u\eta_{k'}\mathbb{E}\left\{\sum_{m=1}^M\sum_{n=1}^M a_{mk}^*\hat{\mathbf{g}}_{mk}^H \mathbf{g}_{mk'}\mathbf{g}_{nk'}^H\hat{\mathbf{g}}_{nk}a_{nk}^T\right\} \\
&= \underbrace{\sum_{k'\in\mathcal{P}_k} p_u\eta_{k'}\mathbb{E}\left\{\sum_{m=1}^M a_{mk}^*\hat{\mathbf{g}}_{mk}^H \mathbf{g}_{mk'}\mathbf{g}_{mk'}^H\hat{\mathbf{g}}_{mk}a_{mk}^T\right\}}_{T_1} \\
&\quad + \underbrace{\sum_{k'\in\mathcal{P}_k} p_u\eta_{k'}\mathbb{E}\left\{\sum_{m=1}^M\sum_{n\neq m} a_{mk}^*\hat{\mathbf{g}}_{mk}^H \mathbf{g}_{mk'}\mathbf{g}_{nk'}^H\hat{\mathbf{g}}_{nk}a_{nk}^T\right\}}_{T2},
\end{aligned}
\tag{60}
$$

The relevant terms in (60) can be given by (61) and (62) at the top of this page.

2) $\sum_{k'\notin\mathcal{P}_k}\mathbb{E}\{|UI_{kk'}|^2\}$: The similar procedure shows that

$$
\begin{aligned}
\sum_{k'\notin\mathcal{P}_k}\mathbb{E}\left\{|UI_{kk'}|^2\right\} &= \underbrace{\sum_{k'\notin\mathcal{P}_k} p_u\eta_{k'}\mathbb{E}\left\{\sum_{m=1}^M a_{mk}^*\hat{\mathbf{g}}_{mk}^H \mathbf{g}_{mk'}\mathbf{g}_{mk'}^H\hat{\mathbf{g}}_{mk}a_{mk}^T\right\}}_{T_3} \\
&\quad + \underbrace{\sum_{k'\notin\mathcal{P}_k} p_u\eta_{k'}\mathbb{E}\left\{\sum_{m=1}^M\sum_{n\neq m} a_{mk}^*\hat{\mathbf{g}}_{mk}^H \mathbf{g}_{mk'}\mathbf{g}_{nk'}^H\hat{\mathbf{g}}_{nk}a_{nk}^T\right\}}_{T4},
\end{aligned}
\tag{63}
$$

where the relevant terms in (63) can be expressed as (64) and (65) at the top of the next page. According to the above-mentioned decomposition, the sum of the inter-user interference can be given by

$$
\begin{aligned}
\sum_{k'=1}^M \mathbb{E}\left\{|UI_{kk'}|^2\right\} &= \sum_{k'\in\mathcal{P}_k} p_u\eta_{k'}\mathbf{a}_k^H \boldsymbol{\Omega}_{kk'}\mathbf{a}_k \\
&\quad + \sum_{k'=1}^K p_u\eta_{k'}\mathbf{a}_k^H\left(\boldsymbol{\Upsilon}_{kk'} + \bar{\boldsymbol{\Upsilon}}_{kk'}\right)\mathbf{a}_k,
\end{aligned}
\tag{66}
$$

where the elements in $\boldsymbol{\Omega}_{kk'} \in \mathbb{C}^{M\times M}$ follow (67) at the top of the next page. Then, $\boldsymbol{\Upsilon}_{kk'} \in \mathbb{C}^{M\times M}$ is a diagonal matrix with its diagonal element satisfies (68) and the elements in $\bar{\boldsymbol{\Upsilon}}_{kk'} \in \mathbb{C}^{M\times M}$ follow (69) at the top of the next page.

D. Compute $\mathbb{E}\{|EMI_k|^2\}$ and $\mathbb{E}\{|NS_k|^2\}$

With the help of (6)-(9), we can decompose the EMI term into (70) at the top of the next page with $\boldsymbol{\Gamma}_{\omega,k} \in \mathbb{C}^{M\times M}$, where

$$
\begin{aligned}
T_3 &= \sum_{k' \notin \mathcal{P}_k} p_u \eta_{k'} a_{mk}^* a_{mk}^T \left\{ \begin{array}{l} \tau_p p_p \mathbb{E}\left\{ \sum_{k'' \in \mathcal{P}_k} \mathbf{g}_{mk''}^H \mathbf{Z}_{mk}^H \mathbf{g}_{mk'} \mathbf{g}_{mk'}^H \mathbf{Z}_{mk} \mathbf{g}_{mk''} \right\} + \mathbb{E}\left\{ (\mathbf{g}_m \bar{\mathbf{\Theta}}_t \mathbf{\Theta}_t \mathbf{N}_t \varphi_k)^H \mathbf{Z}_{mk}^H \mathbf{g}_{mk'} \mathbf{g}_{mk'}^H \mathbf{Z}_{mk} (\mathbf{g}_m \bar{\mathbf{\Theta}}_t \mathbf{\Theta}_t \mathbf{N}_t \varphi_k) \right\} \\ + \mathbb{E}\left\{ (\mathbf{g}_m \bar{\mathbf{\Theta}}_r \mathbf{\Theta}_r \mathbf{N}_r \varphi_k)^H \mathbf{Z}_{mk}^H \mathbf{g}_{mk'} \mathbf{g}_{mk'}^H \mathbf{Z}_{mk} (\mathbf{g}_m \bar{\mathbf{\Theta}}_r \mathbf{\Theta}_r \mathbf{N}_r \varphi_k) \right\} + \mathbb{E}\left\{ (\mathbf{N}_{m,p} \varphi_k)^H \mathbf{Z}_{mk}^H \mathbf{g}_{mk'} \mathbf{g}_{mk'}^H \mathbf{Z}_{mk} (\mathbf{N}_{m,p} \varphi_k) \right\} \end{array} \right\} \\
&= \sum_{k' \notin \mathcal{P}_k} p_u \eta_{k'} a_{mk}^* a_{mk}^T \left\{ \begin{array}{l} \tau_p p_p \sum_{k'' \in \mathcal{P}_k} \beta_m^2 \beta_{k'} \beta_{k''} \left[\mathrm{tr}(\mathbf{R}_{m,r} \mathbf{Z}_{mk}^H \mathbf{R}_{m,r} \mathbf{Z}_{mk}) \mathrm{tr}(\mathbf{T}_{\omega_{k'}}) \mathrm{tr}(\mathbf{T}_{\omega_{k''}}) + \mathrm{tr}(\mathbf{R}_{m,r} \mathbf{Z}_{mk}^H)^2 \mathrm{tr}(\mathbf{T}_{\omega_{k'}} \mathbf{T}_{\omega_{k''}}) \right] \\ + \beta_m^2 \beta_{k'} \sigma_t^2 \left[\mathrm{tr}(\mathbf{R}_{m,r} \mathbf{Z}_{mk}^H \mathbf{R}_{m,r} \mathbf{Z}_{mk}) \mathrm{tr}(\mathbf{T}_{\omega_{k'}}) \mathrm{tr}(\mathbf{T}_t) + \mathrm{tr}(\mathbf{R}_{m,r} \mathbf{Z}_{mk}^H)^2 \mathrm{tr}(\mathbf{T}_{\omega_{k'}} \mathbf{T}_t) \right] \\ + \beta_m^2 \beta_{k'} \sigma_r^2 \left[\mathrm{tr}(\mathbf{R}_{m,r} \mathbf{Z}_{mk}^H \mathbf{R}_{m,r} \mathbf{Z}_{mk}) \mathrm{tr}(\mathbf{T}_{\omega_{k'}}) \mathrm{tr}(\mathbf{T}_r) + \mathrm{tr}(\mathbf{R}_{m,r} \mathbf{Z}_{mk}^H)^2 \mathrm{tr}(\mathbf{T}_{\omega_{k'}} \mathbf{T}_r) \right] + \sigma^2 \mathrm{tr}\left(\mathbf{\Delta}_{mk'} \mathbf{Z}_{mk} \mathbf{Z}_{mk}^H \right) \end{array} \right\},
\end{aligned}
\tag{64}
$$

$$
\begin{aligned}
T_4 &= \sum_{k' \notin \mathcal{P}_k} p_u \eta_{k'} \sum_{m=1}^M \sum_{n \neq m} a_{mk}^* a_{nk}^T \left\{ \begin{array}{l} \tau_p p_p \mathbb{E}\left\{ \sum_{k'' \in \mathcal{P}_k} \mathbf{g}_{mk''}^H \mathbf{Z}_{mk}^H \mathbf{g}_{mk'} \mathbf{g}_{nk'}^H \mathbf{Z}_{nk} \mathbf{g}_{nk''} \right\} + \mathbb{E}\left\{ (\mathbf{g}_m \bar{\mathbf{\Theta}}_t \mathbf{\Theta}_t \mathbf{N}_t \varphi_k)^H \mathbf{Z}_{mk}^H \mathbf{g}_{mk'} \mathbf{g}_{nk'}^H \mathbf{Z}_{nk} (\mathbf{g}_n \bar{\mathbf{\Theta}}_t \mathbf{\Theta}_t \mathbf{N}_t \varphi_k) \right\} \\ + \mathbb{E}\left\{ (\mathbf{g}_m \bar{\mathbf{\Theta}}_r \mathbf{\Theta}_r \mathbf{N}_r \varphi_k)^H \mathbf{Z}_{mk}^H \mathbf{g}_{mk'} \mathbf{g}_{nk'}^H \mathbf{Z}_{nk} (\mathbf{g}_n \bar{\mathbf{\Theta}}_r \mathbf{\Theta}_r \mathbf{N}_r \varphi_k) \right\} + \mathbb{E}\left\{ (\mathbf{N}_{m,p} \varphi_k)^H \mathbf{Z}_{mk}^H \mathbf{g}_{mk'} \mathbf{g}_{mk'}^H \mathbf{Z}_{nk} (\mathbf{N}_{n,p} \varphi_k) \right\} \end{array} \right\} \\
&= \sum_{k' \notin \mathcal{P}_k} p_u \eta_{k'} \sum_{m=1}^M \sum_{n \neq m} a_{mk}^* a_{nk}^T \left\{ \begin{array}{l} \tau_p p_p \sum_{k'' \in \mathcal{P}_k} \beta_m \beta_n \beta_{k'} \beta_{k''} \mathrm{tr}(\mathbf{R}_{m,r} \mathbf{Z}_{mk}^H) \mathrm{tr}(\mathbf{R}_{n,r} \mathbf{Z}_{nk}) \mathrm{tr}(\mathbf{T}_{\omega_{k'}} \mathbf{T}_{\omega_{k''}}) \\ + \beta_m \beta_n \beta_{k'} \mathrm{tr}(\mathbf{R}_{m,r} \mathbf{Z}_{mk}^H) \mathrm{tr}(\mathbf{R}_{n,r} \mathbf{Z}_{nk}) \left[\sigma_t^2 \mathrm{tr}(\mathbf{T}_{\omega_{k'}} \mathbf{T}_t) + \sigma_r^2 \mathrm{tr}(\mathbf{T}_{\omega_{k'}} \mathbf{T}_r) \right] \end{array} \right\}.
\end{aligned}
\tag{65}
$$

$$
[\mathbf{\Omega}_{kk'}]_{mn} = \left\{ \begin{array}{ll} \tau_p p_p (\beta_m \beta_{k'})^2 \left[\mathrm{tr}(\mathbf{T}_{\omega_{k'}})^2 \mathrm{tr}(\mathbf{R}_{m,r} \mathbf{Z}_{mk}^H)^2 + \mathrm{tr}(\mathbf{T}_{\omega_{k'}}^2) \mathrm{tr}(\mathbf{R}_{m,r} \mathbf{Z}_{mk}^H \mathbf{R}_{m,r} \mathbf{Z}_{mk}) \right], & m = n \\ \tau_p p_p \beta_m \beta_n \beta_{k'}^2 \mathrm{tr}(\mathbf{R}_{m,r} \mathbf{Z}_{mk}^H) \mathrm{tr}(\mathbf{R}_{n,r} \mathbf{Z}_{nk}) \mathrm{tr}(\mathbf{T}_{\omega_{k'}})^2, & m \neq n \end{array} \right.
\tag{67}
$$

$$
[\mathbf{\Upsilon}_{kk'}]_{mm} = \left[\tau_p p_p \sum_{k'' \in \mathcal{P}_k} \beta_m^2 \beta_{k'} \beta_{k''} \mathrm{tr}(\mathbf{T}_{\omega_{k'}}) \mathrm{tr}(\mathbf{T}_{\omega_{k''}}) + \beta_m^2 \beta_{k'} \left(\sigma_t^2 \mathrm{tr}(\mathbf{T}_t) + \sigma_r^2 \mathrm{tr}(\mathbf{T}_r) \right) \mathrm{tr}(\mathbf{T}_{\omega_{k'}}) \right] \mathrm{tr}(\mathbf{R}_{m,r} \mathbf{Z}_{mk}^H \mathbf{R}_{m,r} \mathbf{Z}_{mk}) + \sigma^2 \mathrm{tr}\left(\mathbf{\Delta}_{mk'} \mathbf{Z}_{mk} \mathbf{Z}_{mk}^H \right),
\tag{68}
$$

$$
[\bar{\mathbf{\Upsilon}}_{kk'}]_{mn} = \left[\tau_p p_p \sum_{k'' \in \mathcal{P}_k} \beta_m \beta_n \beta_{k'} \beta_{k''} \mathrm{tr}(\mathbf{T}_{\omega_{k'}} \mathbf{T}_{\omega_{k''}}) + \beta_m \beta_n \beta_{k'} \left(\sigma_t^2 \mathrm{tr}(\mathbf{T}_t \mathbf{T}_{\omega_{k'}}) + \sigma_r^2 \mathrm{tr}(\mathbf{T}_r \mathbf{T}_{\omega_{k'}}) \right) \right] \mathrm{tr}(\mathbf{R}_{m,r} \mathbf{Z}_{mk}^H) \mathrm{tr}(\mathbf{R}_{n,r} \mathbf{Z}_{nk}).
\tag{69}
$$

$$
\begin{aligned}
&\mathbb{E}\left\{ \left| \sum_{m=1}^M a_{mk}^* \hat{\mathbf{g}}_{mk}^H \mathbf{g}_m \bar{\mathbf{\Theta}}_\omega \mathbf{\Theta}_\omega \mathbf{n}_\omega \right|^2 \right\} \\
&= \mathbb{E}\left\{ \sum_{m=1}^M a_{mk}^* \hat{\mathbf{g}}_{mk}^H \mathbf{g}_m \bar{\mathbf{\Theta}}_\omega \mathbf{\Theta}_\omega \mathbf{n}_\omega \mathbf{n}_\omega^H \mathbf{\Theta}_\omega^H \bar{\mathbf{\Theta}}_\omega^H (\mathbf{g}_m)^H \hat{\mathbf{g}}_{mk} a_{mk}^T \right\} + \mathbb{E}\left\{ \sum_{m=1}^M \sum_{n \neq m} a_{mk}^* \hat{\mathbf{g}}_{mk}^H \mathbf{g}_m \bar{\mathbf{\Theta}}_\omega \mathbf{\Theta}_\omega \mathbf{n}_\omega \mathbf{n}_\omega^H \mathbf{\Theta}_\omega^H \bar{\mathbf{\Theta}}_\omega^H (\mathbf{g}_n)^H \hat{\mathbf{g}}_{nk} a_{nk}^T \right\} \\
&= \sum_{m=1}^M a_{mk}^* \sigma_\omega^2 \mathrm{tr}(\mathbf{T}_\omega) \left\{ (\beta_m)^2 \left[\tau_p p_p \sum_{k' \in \mathcal{P}_k} \beta_{k'} \mathrm{tr}(\mathbf{T}_{\omega_{k'}}) + \left(\sigma_r^2 \mathrm{tr}(\mathbf{T}_r) + \sigma_t^2 \mathrm{tr}(\mathbf{T}_t) \right) \right] \mathrm{tr}\left(\mathbf{R}_{m,r} \mathbf{Z}_{mk}^H \mathbf{R}_{m,r} \mathbf{Z}_{mk} \right) + \beta_m \sigma^2 \mathrm{tr}\left(\mathbf{Z}_{mk}^H \mathbf{R}_{m,r} \mathbf{Z}_{mk} \right) \right\} a_{mk}^T \\
&\quad + \sum_{m=1}^M \sum_{n=1}^M a_{mk}^* \sigma_\omega^2 \left\{ \beta_m \beta_n \mathrm{tr}(\mathbf{R}_{m,r} \mathbf{Z}_{mk}^H) \mathrm{tr}(\mathbf{R}_{n,r} \mathbf{Z}_{nk}) \left[\tau_p p_p \sum_{k' \in \mathcal{P}_k} \beta_{k'} \mathrm{tr}(\mathbf{T}_{\omega_{k'}} \mathbf{T}_\omega) + \sigma_r^2 \mathrm{tr}(\mathbf{T}_r \mathbf{T}_\omega) + \sigma_t^2 \mathrm{tr}(\mathbf{T}_t \mathbf{T}_\omega) \right] \right\} a_{nk}^T \\
&= \sigma_\omega^2 \mathbf{a}_k^H \mathbf{\Gamma}_{\omega,k} \mathbf{a}_k,
\end{aligned}
\tag{70}
$$

the diagonal elements $\gamma_{\omega,mmk}$ in $\mathbf{\Gamma}_{\omega,k}$ follow (71) and the other elements $\gamma_{\omega,mnk}$, $m \neq n$ follow (72) at the top of the next page. Finally, we can compute the noise power directly by

$$
\begin{aligned}
\mathbb{E}\{|\mathrm{NS}_k|^2\} &= \mathbb{E}\left\{ \left| \sum_{m=1}^M a_{mk}^* \hat{\mathbf{g}}_{mk}^H \mathbf{w}_m \right|^2 \right\} \\
&= \mathbb{E}\left\{ \sum_{m=1}^M a_{mk}^* \hat{\mathbf{g}}_{mk}^H \mathbf{w}_m \mathbf{w}_m^H \hat{\mathbf{g}}_{mk} a_{mk}^T \right\} \\
&= \sum_{m=1}^M \sigma^2 a_{mk}^* \mathrm{tr}(\mathbf{Q}_{mk}) a_{mk}^T \\
&= \sigma^2 \mathbf{a}_k^H \mathbf{\Lambda}_k \mathbf{a}_k,
\end{aligned}
\tag{73}
$$

where $\mathbf{\Lambda}_k = \mathrm{diag}(\mathbf{b}_k) \in \mathbb{C}^{M \times M}$, and this finishes the proof.

REFERENCES

[1] X. Mu *et al.*, "Simultaneously transmitting and reflecting (STAR) RIS aided wireless communications," *IEEE Trans. Wireless Commun.*, vol. 21, no. 5, pp. 3083–3098, 2022.

[2] H. Q. Ngo *et al.*, "Cell-free massive MIMO versus small cells," *IEEE Trans. Wireless Commun.*, vol. 16, no. 3, pp. 1834–1850, 2017.

[3] T. Van Chien *et al.*, "Reconfigurable intelligent surface-assisted cell-free massive MIMO systems over spatially-correlated channels," *IEEE Trans. Wireless Commun.*, vol. 21, no. 7, pp. 5106–5128, 2022.

[4] K. B. Letaief *et al.*, "The roadmap to 6G: AI empowered wireless networks," *IEEE Commun. Mag.*, vol. 57, no. 8, pp. 84–90, 2019.

[5] A. Papazafeiropoulos *et al.*, "STAR-RIS assisted cell-free massive MIMO system under spatially-correlated channels," *IEEE Trans. Veh. Tech.*, pp. 1–16, 2023.

[6] Y. Zhang *et al.*, "Performance analysis of RIS-assisted cell-free massive MIMO systems with transceiver hardware impairments," *IEEE Trans. Commun.*, pp. 1–1, 2023.

[7] E. Shi *et al.*, "Uplink performance of RIS-aided cell-free massive MIMO system with electromagnetic interference," *IEEE J. Sel. Areas Commun.*, vol. 41, no. 8, pp. 2431–2445, 2023.

[8] X. Ma *et al.*, "Cooperative beamforming for RIS-aided cell-free massive MIMO networks," *IEEE Trans. Wireless Commun.*, vol. 22, no. 11, pp. 7243–7258, 2023.

[9] J. Zheng *et al.*, "Mobile cell-free massive MIMO: Challenges, solutions, and future directions," *IEEE Wireless Commun.*, vol. 31, no. 3, pp. 140–147, 2024.

[10] P. Biswas *et al.*, "Optimal access point centric clustering for cell-free massive MIMO using gaussian mixture model clustering," *IEEE trans.*

$$
\begin{aligned}
\gamma_{\omega,mmk} &= \mathrm{tr}(\mathbf{T}_\omega)\Bigg\{(\beta_m)^2\Big[\tau_p p_p \sum_{k'\in\mathcal{P}_k}\beta_{k'}\mathrm{tr}(\mathbf{T}_{\omega_{k'}}) + \sigma_r^2\mathrm{tr}(\mathbf{T}_r) + \sigma_t^2\mathrm{tr}(\mathbf{T}_t)\Big]\mathrm{tr}\left(\mathbf{R}_{m,r}\mathbf{Z}_{mk}^H\mathbf{R}_{m,r}\mathbf{Z}_{mk}\right) + \beta_m\sigma^2\mathrm{tr}\left(\mathbf{Z}_{mk}^H\mathbf{R}_{m,r}\mathbf{Z}_{mk}\right)\Bigg\} \\
&\quad + \beta_m^2\mathrm{tr}(\mathbf{R}_{m,r}\mathbf{Z}_{mk}^H)\mathrm{tr}(\mathbf{R}_{m,r}\mathbf{Z}_{mk})\Big[\tau_p p_p \sum_{k'\in\mathcal{P}_k}\beta_{k'}\mathrm{tr}(\mathbf{T}_{\omega_{k'}}\mathbf{T}_\omega) + \sigma_r^2\mathrm{tr}(\mathbf{T}_r\mathbf{T}_\omega) + \sigma_t^2\mathrm{tr}(\mathbf{T}_t\mathbf{T}_\omega)\Big],
\end{aligned}
\tag{71}
$$

$$
\gamma_{\omega,mnk} = \beta_m\beta_n\mathrm{tr}(\mathbf{R}_{m,r}\mathbf{Z}_{mk}^H)\mathrm{tr}(\mathbf{R}_{n,r}\mathbf{Z}_{nk})\Big[\tau_p p_p \sum_{k'\in\mathcal{P}_k}\beta_{k'}\mathrm{tr}(\mathbf{T}_{\omega_{k'}}\mathbf{T}_\omega) + \sigma_r^2\mathrm{tr}(\mathbf{T}_r\mathbf{T}_\omega) + \sigma_t^2\mathrm{tr}(\mathbf{T}_t\mathbf{T}_\omega)\Big].
\tag{72}
$$

Mach. Learn. Commun. Netw., vol. 2, pp. 675–687, 2024.

[11] E. Nayebi *et al.*, "Precoding and power optimization in cell-free massive MIMO systems," *IEEE Trans. Wireless Commun.*, vol. 16, no. 7, pp. 4445–4459, 2017.

[12] J. Zheng *et al.*, "Impact of channel aging on cell-free massive MIMO over spatially correlated channels," *IEEE Trans. Wireless Commun.*, vol. 20, no. 10, pp. 6451–6466, 2021.

[13] J. Qian *et al.*, "Impact of channel aging and electromagnetic interference on RIS-assisted cell-free massive MIMO systems," 2024. [Online]. Available: https://arxiv.org/abs/2407.03785

[14] Q. Wu *et al.*, "Intelligent reflecting surface-aided wireless communications: A tutorial," *IEEE Trans. Commun.*, vol. 69, no. 5, pp. 3313–3351, 2021.

[15] Y. Zhang *et al.*, "Channel aging-aware precoding for RIS-aided multi-user communications," *IEEE Trans. Veh. Technol.*, vol. 72, no. 2, pp. 1997–2008, 2023.

[16] A. Papazafeiropoulos *et al.*, "Impact of channel aging on reconfigurable intelligent surface aided massive MIMO systems with statistical CSI," *IEEE Trans. Veh. Technol.*, vol. 72, no. 1, pp. 689–703, 2023.

[17] J. Zuo *et al.*, "Joint design for simultaneously transmitting and reflecting (STAR) RIS assisted NOMA systems," *IEEE Trans. Wireless Commun.*, vol. 22, no. 1, pp. 611–626, 2023.

[18] M. Bashar *et al.*, "On the performance of reconfigurable intelligent surface-aided cell-free massive MIMO uplink," in *Proc. IEEE GLOBECOM*, 2020, pp. 1–6.

[19] E. Shi *et al.*, "Uplink performance of RIS-aided cell-free massive MIMO system over spatially correlated channels," in *Proc. IEEE GLOBECOM*, 2022, pp. 3259–3264.

[20] ——, "RIS-aided cell-free massive MIMO systems for 6G: Fundamentals, system design, and applications," *Proc. IEEE*, vol. 112, no. 4, pp. 331–364, 2024.

[21] X. Ma *et al.*, "Active STAR-RIS aided cell-free massive MIMO: A performance study," *IEEE Trans. Veh. Technol.*, pp. 1–6, 2023.

[22] J. Qian *et al.*, "Two-phase channel estimation for RIS-aided cell-free massive MIMO with electromagnetic interference," in *Proc. IEEE MeditCom*, 2024, pp. 471–476.

[23] Y. Zhang *et al.*, "Beyond cell-free MIMO: Energy efficient reconfigurable intelligent surface aided cell-free MIMO communications," *IEEE Trans. Cogn. Commun. Netw.*, vol. 7, no. 2, pp. 412–426, 2021.

[24] Y. Song *et al.*, "Weighted sum-rate maximization for multi-STAR-RIS-assisted mmwave cell-free networks," *IEEE Trans. Veh. Tech.*, vol. 73, no. 4, pp. 5304–5320, 2024.

[25] J. Xu *et al.*, "STAR-RISs: Simultaneous transmitting and reflecting reconfigurable intelligent surfaces," *IEEE Commun. Lett.*, vol. 25, no. 9, pp. 3134–3138, 2021.

[26] Y. Liu *et al.*, "STAR: Simultaneous transmission and reflection for 360° coverage by intelligent surfaces," *IEEE Wireless Commun.*, vol. 28, no. 6, pp. 102–109, 2021.

[27] A. Papazafeiropoulos *et al.*, "Coverage probability of STAR-RIS-assisted massive MIMO systems with correlation and phase errors," *IEEE Wireless Commun. Lett.*, vol. 11, no. 8, pp. 1738–1742, 2022.

[28] C. Wu *et al.*, "Coverage characterization of STAR-RIS networks: NOMA and OMA," *IEEE Commun. Lett.*, vol. 25, no. 9, pp. 3036–3040, 2021.

[29] ——, "Resource allocation in STAR-RIS-aided networks: OMA and NOMA," *IEEE Trans. Wireless Commun.*, vol. 21, no. 9, pp. 7653–7667, 2022.

[30] F. Karim *et al.*, "STAR-RIS aided full duplex communication system: Performance analysis," in *Proc. IEEE GLOBECOM*, 2022, pp. 3114–3119.

[31] H. Ge *et al.*, "Impact of phase noise in downlink STAR-RIS-aided massive MIMO systems," *IEEE Commun. Lett.*, vol. 28, no. 2, pp. 392–396, 2024.

[32] M.-A. Badiu and J. P. Coon, "Communication through a large reflecting surface with phase errors," *IEEE Wireless Commun. Lett.*, vol. 9, no. 2, pp. 184–188, 2020.

[33] A. Papazafeiropoulos *et al.*, "Intelligent reflecting surface-assisted MU-MISO systems with imperfect hardware: Channel estimation and beamforming design," *IEEE Trans. Wireless Commun.*, vol. 21, no. 3, pp. 2077–2092, 2022.

[34] S. Hassouna *et al.*, "Reconfigurable intelligent surfaces aided wireless communications with electromagnetic interference," in *Proc. IEEE EuCAP*, 2023, pp. 1–5.

[35] A. de Jesus Torres *et al.*, "Electromagnetic interference in RIS-aided communications," *IEEE Wireless Commun. Lett.*, vol. 11, no. 4, pp. 668–672, 2022.

[36] J. Qian *et al.*, "The effect of spatial correlation and mutual coupling on cell-free massive MIMO," in *Proc. IEEE WCNC*, 2024, pp. 01–06.

[37] Q. Li *et al.*, "Performance analysis of active RIS-aided systems in the face of imperfect CSI and phase shift noise," *IEEE Trans. Veh. Tech.*, vol. 72, no. 6, pp. 8140–8145, 2023.

[38] E. Björnson and L. Sanguinetti, "Rayleigh fading modeling and channel hardening for reconfigurable intelligent surfaces," *IEEE Wireless Commun. Lett.*, vol. 10, no. 4, pp. 830–834, 2021.

[39] J. Qian *et al.*, "Partial CSI acquisition for size-constrained massive MIMO systems with user mobility," *IEEE Trans. Veh. Technol.*, vol. 67, no. 9, pp. 9016–9020, 2018.

[40] J.-C. Chen and Y.-C. Lin, "A projected gradient descent algorithm for designing low-resolution finite-alphabet equalizers in all-digital massive MU-MIMO communication systems," *IEEE Access*, vol. 11, pp. 50 744–50 751, 2023.

[41] A. Abdallah and M. M. Mansour, "Efficient angle-domain processing for FDD-based cell-free massive MIMO systems," *IEEE Trans. Commun.*, vol. 68, no. 4, pp. 2188–2203, 2020.

[42] A. Papazafeiropoulos *et al.*, "Cooperative RIS and STAR-RIS assisted mMIMO communication: Analysis and optimization," *IEEE Trans. Veh. Tech.*, vol. 72, no. 9, pp. 11 975–11 989, 2023.

[43] R. Ranjan *et al.*, "A gradient ascent based low complexity rate maximization algorithm for intelligent reflecting surface-aided OFDM systems," *IEEE Commun. Lett.*, vol. 27, no. 8, pp. 2083–2087, 2023.

[44] P. Nuti and B. L. Evans, "Spectral efficiency vs complexity in downlink algorithms for reconfigurable intelligent surfaces," in *Proc. IEEE ICC*, 2021, pp. 1–7.

[45] T. P. Minka, "Old and new matrix algebra useful for statistics," 2000. [Online]. Available: https://api.semanticscholar.org/CorpusID:15971655

[46] A. Hjorungnes and D. Gesbert, "Complex-valued matrix differentiation: Techniques and key results," *IEEE Tran. Signal Proc.*, vol. 55, no. 6, pp. 2740–2746, 2007.

[47] E. Björnson and L. Sanguinetti, "Making cell-free massive MIMO competitive with MMSE processing and centralized implementation," *IEEE Trans. Wireless Commun.*, vol. 19, no. 1, pp. 77–90, 2020.

[48] R. Nikbakht *et al.*, "Uplink fractional power control and downlink power allocation for cell-free networks," *IEEE Wireless Commun. Lett.*, vol. 9, no. 6, pp. 774–777, 2020.

[49] C. Wu *et al.*, "Channel estimation for STAR-RIS-aided wireless communication," *IEEE Commun. Lett.*, vol. 26, no. 3, pp. 652–656, 2022.

[50] S. Loyka, "Channel capacity of MIMO architecture using the exponential correlation matrix," *IEEE Commun. Lett.*, vol. 5, no. 9, pp. 369–371, 2001.

[51] A. Hjørungnes, *Complex-Valued Matrix Derivatives: With Applications in Signal Processing and Communications*. Cambridge University Press, 2011.

[52] H. Fang *et al.*, "On the performance of RIS-aided cell-free massive MIMO systems under channel aging," *IEEE Trans. Veh. Tech.*, pp. 1–14, 2024.